SCIENCE OF LIGHT

VOLUME 7 NUMBER 2

August

1958

Published by the

Institute for Optical Research

Tokyo University of Education

in collaboration with

The Spectroscopical Society of Japan

SCIENCE OF LIGHT

Science of Light contains reports of the Institute for Optical Research and contribution from other science bodies about similar subjects.

The editorial staff consists of following members:

All communications should be addressed to the director or to the librarian of the Institute.

The Institute for Optical Research

Tokyo University of Education

400, 4-chome, Hyakunin-machi, Shinjuku-ku, Tokyo, Japan

Printed at
the Printing Department, Chūō Kagakusha,
Tokyo

Grating Mounting for Vacuum Ultraviolet Monochromator

Ryumyo ONAKA

Institute for Optical Research, Tokyo University of Education, Shinjuku-ku, Tokyo

(Received July 10, 1958)

Abstract

Use of rotation of a concave grating about a point displaced from the center of the grating found by P. D. Johnson is applicable not only to a near Eagle mounting (angle of deflection $\approx \pi$) but also to a monochromator of any angle of deflection. A generalized analysis is given to the grating mounting of this type, and it is shown that the mounting is useful for a monochromator in the near vacuum ultraviolet region.

1. Introduction

There have been reported several methods of mounting concave diffraction gratings in vacuum ultraviolet monochromators. Mounting of a concave grating on the end of an arm pivoted at the center of the Rowland circle, reported by Fujioka and Ito[1], and Tousey, Johnson, Richardson and Toran[2] secures perfect focus for any wavelength, but has a disadvantage of changing the emerging direction of monochromatic radiation from the exit slit. Simple rotation of the concave grating about its center is also used when the resolution is not essential requirement as in the spectrophotometric studies in solid or liquid materials. An improved mounting of this type was found by M. Seya[3], and discussed in detail by Greiner and Schäffer[4]. In Seya mounting the angle between incidence and diffracted light has a special value, namely 70°15′, and good focus is obtained over a wide wavelength range. Recently another method of extention of the available wavelength range was reported by P. D. Johnson[5], who used rotation of the concave gration about a point displaced from the center of the grating. Though his analysis of the mounting was carried out for only near Eagle mounting (angle of deflection $\approx \pi$), his mounting seems to be applicable for any angle of deflection. Practically the two slits of a monochramator can not be made so close as in the Eagle mounting, and therefore a generalized analysis of the mounting of this type for any angle of deflection would be worth to be studied.

1) Fujioka and Ito, Science of Light, **1** (1951) 1.
2) Tousey, Johnson, Richardson and Toran, J. Opt. Soc. Am., **41** (1951) 696.
3) M. Seya, Science of Light, **2** (1952) 8.
4) Greiner and Schäffer, Optik **14** (1957) 263, **15** (1958) 51.
5) P. D. Johnson, Rev. Sci. Inst. **28** (1957) 833.

2. Rotation of a Concave Grating about the Axis Displaced from the Grating Center

In general a concave grating gives a perfect focus when Rowland conditions are fulfilled, but rotation of the grating from this position makes the focus blurred. The problem we are now faced is how to prevent this defocusing.

In analysing the mounting of concave grating, it is convenient to use Beutler's equation for focusing[6],

$$\left|\frac{A}{2}W^2+\frac{B}{2}W^3+\cdots\cdots\right|\leq\frac{\lambda}{4}, \tag{1}$$

$$\left.\begin{aligned} A&=\frac{\cos^2\alpha}{r}-\frac{\cos\alpha}{R}+\frac{\cos^2\beta}{r'}-\frac{\cos\beta}{R},\\ B&=\frac{\sin\alpha}{r}\left(\frac{\cos^2\alpha}{r}-\frac{\cos\alpha}{R}\right)+\frac{\sin\beta}{r'}\left(\frac{\cos^2\beta}{r'}-\frac{\cos\beta}{R}\right),\end{aligned}\right\} \tag{2}$$

where W: half of the width of the grating,
α: angle of incidence,
β: angle of diffraction,
r: distance from the entrance slit to the center of the grating,
r': distance from the exit slit to the center of the grating,
R: diameter of the Rowland circle.

The left hand side of the equation (1) devided by $\left(\frac{\lambda}{2\pi}\right)$ gives the phase difference between the rays that pass the center and the edge of the grating. Rowland circule conditions are

$$\frac{\cos\alpha}{r}-\frac{1}{R}=0 \text{ and } \frac{\cos\beta}{r'}-\frac{1}{R}=0, \tag{3}$$

which give exactly $A=B=0$ and, therefore, the focusing is perfect. But if the grating is rotated by a small angle δ, $A\neq0$, $B\neq0$ in general, both A and B being possible to be expanded in power series of δ starting by δ^1. The main cause of defocusing will then be δ^1 term in A, and the next δ^2 term in A or δ_1 term in B. By using an appropriate position of pivoting, δ^1 term in A will vanish, leaving only those defocusing terms of comparatively small significance.

Fig. 1 shows the optical arrangements in which S_1 denotes the entrance slit, S_2 the exit, $G(G_0)$ the position of the center of grating, C, the pivoting point of of the grating, M_1 and M_2 midway points of the Rowland circle between S_1 and S_2 $O(O_0)$ the center of the Rowland circle, $\alpha(\alpha_0)$ the angle of incidence, $\beta(\beta_0)$ the angle of diffraction.

6) H. G. Beutler, J. Opt. Soc. Am. **35** (1945) 311.

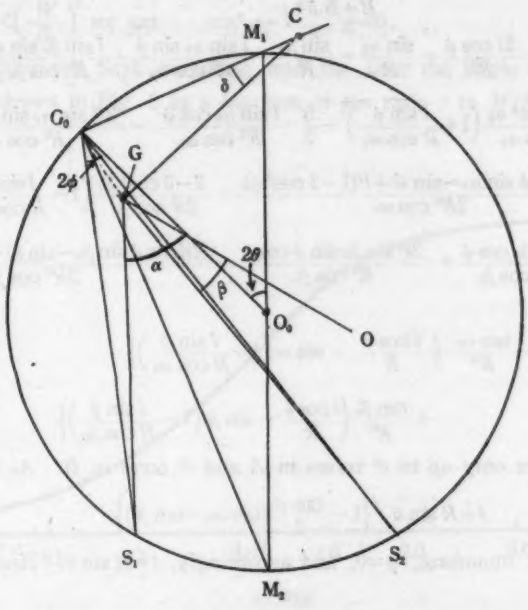

Fig. 1. Optical arrangement of the monochromator.

Suffix $_0$ indicates the states before the grating is rotated, fulfiling Rowland circle conditions.

Let $l=\overline{G_0C}$, $2\theta=\angle M_1O_0G_0$, $2\phi=\angle S_1G_0S_2$, then, $\alpha_0=\theta+\phi$, $\beta_0=\theta-\phi$.

To reduce the amount of changes in incident and emerging directions, the center of rotation is brought on the line $\overline{G_0C}$ and the grating is moved toward M_2 for a small δ.

By expanding α, β, $1/r$ and $1/r'$ in power series of δ, we get

$$\left.\begin{aligned}\alpha&=\alpha_0+\left(1+\frac{l\sin\phi}{R\cos\alpha_0}\right)\delta+\left(\frac{l\cos\phi}{2R\cos\alpha_0}+\frac{l^2\cos\phi\sin\phi}{R^2\cos^2\alpha_0}\right)\delta^2+\cdots\cdots\\ \beta&=\beta_0+\left(1-\frac{l\sin\phi}{R\cos\beta_0}\right)\delta+\left(\frac{l\cos\phi}{2R\cos\beta_0}-\frac{l^2\cos\phi\sin\phi}{R^2\cos^2\beta_0}\right)\delta^2+\cdots\cdots\end{aligned}\right\}\tag{4}$$

$$\left.\begin{aligned}\frac{1}{r}&=\frac{1}{R\cos\alpha_0}\left[1+\frac{l\cos\phi}{R\cos\alpha_0}\delta-\frac{Rl(\cos\phi\sin\alpha_0-\sin\theta)+l^2(1-3\cos^2\phi)}{2R^2\cos^2\alpha_0}\delta^2+\cdots\cdots\right.\\ \frac{1}{r'}&=\frac{1}{R\cos\beta_0}\left[1+\frac{l\cos\phi}{R\cos\beta_0}\delta-\frac{Rl(\cos\phi\sin\beta_0-\sin\theta)+l^2(1-3\cos^2\phi)}{2R^2\cos^2\beta_0}\delta^2+\cdots\cdots\right.\end{aligned}\right\}\tag{5}$$

After elementary calcutions we have

$$A=A_1\delta+A_2\delta^2+\cdots\cdots,\tag{6}$$

$$B=B_1\delta+\cdots\cdots, \tag{7}$$

where $$A_1=\frac{2l\cos\phi}{R^2}-\frac{\sin\alpha_0}{R}-\frac{\sin\beta_0}{R}-\frac{l\sin\alpha_0\sin\phi}{R^2\cos\alpha_0}+\frac{l\sin\beta_0\sin\phi}{R^2\cos\beta_0}, \tag{8}$$

$$A_2=\frac{2-3\cos^2\alpha_0}{2R\cos\alpha_0}\left(1+\frac{l\sin\phi}{R\cos\alpha_0}\right)^2-\frac{5}{2}\frac{l\sin\alpha_0\cos\phi}{R^2\cos\alpha_0}-\frac{3l^2\sin\alpha_0\sin\phi\cos\phi}{R^3\cos\alpha_0}$$
$$-\frac{Rl(\cos\phi\sin\alpha_0-\sin\theta)+l^2(1-3\cos^2\phi)}{2R^3\cos\alpha_0}+\frac{2-3\cos^2\beta_0}{2R\cos\beta_0}\left(1-\frac{l\sin\phi}{R\cos\phi_0}\right)^2$$
$$-\frac{5}{2}\frac{l\sin\beta_0\cos\phi}{R^2\cos\beta_0}+\frac{3l^2\sin\beta_0\sin\phi\cos\phi}{R^3\cos\beta_0}-\frac{Rl(\cos\phi\sin\beta_0-\sin\theta)+l^2(1-3\cos^2\phi)}{2R^3\cos\beta_0} \tag{9}$$

$$B_1=\frac{\tan\alpha_0}{R^2}\left\{\frac{l\cos\phi}{R}-\sin\alpha_0\left(1+\frac{l\sin\phi}{R\cos\alpha_0}\right)\right\}$$
$$+\frac{\tan\beta_0}{R^2}\left\{\frac{l\cos\phi}{R}-\sin\beta_0\left(1-\frac{l\sin\phi}{R\cos\beta_0}\right)\right\}. \tag{10}$$

Here we consider only up to δ^2 terms in A and δ^1 term in B. A_1 vanishes with

$$l=R\sin\theta\Big/\left\{1-\frac{\tan\phi}{2}(\tan\alpha_0-\tan\beta_0)\right\}. \tag{11}$$

For near Eagle mounting, $\phi\approx0$, and accordingly, $l=R\sin\theta$. Hence C coincides with M_1.

3. Discussion

Though there remain still higher order terms A_2, B_1 etc., after the vanishing A_1 by using an appropriate l, we have another degree of freedom, arbitrariness of ϕ. For short wavelength radiations, $\theta\approx0$, $l\approx0$, $\alpha\approx-\beta\approx\phi$, and therefore

$$\left.\begin{aligned}A_2&=(2-3\cos^2\phi)/R\cos\phi,\\ B_1&=-(2-2\cos^2\phi)/R^2\cos\phi.\end{aligned}\right\} \tag{12}$$

Beutler's equation then becomes,

$$\left|\frac{W^2\delta}{2R}\left(\frac{2-3\cos^2\phi}{\cos\phi}\delta-\frac{2-2\cos^2\phi}{\cos\phi}\cdot\frac{W}{R}\right)\right|\leq\frac{\lambda}{4}, \tag{13}$$

To find ϕ which minimizes the left hand side for both signs of W, we put

$$\frac{\partial}{\partial\phi}\left\{\left(\frac{2-3\cos^2\phi}{\cos\phi}\delta\right)^2+\left(\frac{2-2\cos^2\phi}{\cos\phi}\cdot\frac{W}{R}\right)^2\right\}=0, \tag{14}$$

then we get

$$\cos^4\phi=\frac{\delta^2+\left(\frac{W}{R}\right)^2}{\frac{9}{4}\delta^2+\left(\frac{W}{R}\right)^2}.$$

As extreme cases

for $\delta^2>\left(\frac{W}{R}\right)^2$ we get $\quad\cos^4\phi=\frac{4}{9}\quad$ or $\phi=35°16'$,

for $\delta^2 < \left(\frac{W}{R}\right)^2$ we get $\cos^4\phi = 1$ $\phi = 0$.

The former gives the Seya mounting and the later the Eagle mounting. The optimum ϕ is shown in Fig. 2 as a function of the ratio δ to W/R.

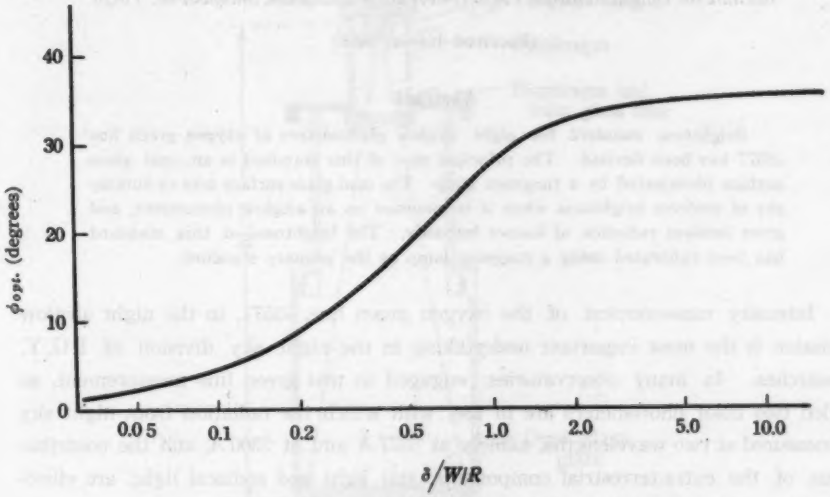

Fig. 2. Optimum value of ϕ as a function of the ratio, δ to W/R.

As a typical example, take the case, $R=40$ cm, 600 grooves/mm, $\lambda_0=1500$ A, $\phi=15°$. Then $\alpha_0=17°40'$, $\beta_0=-12°20'$, and we get

$$l=2,008 \text{ cm},$$

and

$$A_2=-2,075\times10^{-2}\text{ cm}^{-1},$$

$$B_1=-8.73\times10^{-5}\text{ cm}^{-2}.$$

The available wavelength range calculated from Rayleigh criterion is then,

$$-5.67\times10^{-3}<\delta<1.327\times10^{-2},$$

or

$$1317\text{ A}<\lambda<1928\text{ A}.$$

Rayleigh criterion is sometimes too severe to be practical, especially for shorter wavelengths. If we use slits of $2w$ in width, $\lambda/4$ in equation (1) should be replaced by $\frac{wW}{4R}$. Then we get

for 10 μ slits $|\delta|<1.37\times10^{-2}$, or $1060\text{ A}<\lambda<1940\text{ A}$,

for 40 μ slits $|\delta|<3.08\times10^{-2}$, or $510\text{ A}<\lambda<2490\text{ A}$.

These limits show that the focusing of the monochromator may be adequate for spectrophotometry in the near vacuum ultraviolet region.

The author wishes to thank Prof. K. P. Miyake for his kind advise, and to Mr. I. Fujita for his kindness in checking the calculations.

Brightness Standard for Night Airglow Photometers of OI λ5577

Ryumyo ONAKA and Masatoshi NAKAMURA

Institute for Optical Research, Tokyo University of Education, Shinjuku-ku, Tokyo

(Received July 4, 1958)

Abstract

Brightness standard for night airglow photometers of oxygen green line λ5577 has been devised. The principal part of this standard is an opal glass surface illuminated by a tungsten lamp. The opal glass surface acts as dummy sky of uniform brightness when it is mounted on an airglow photometer, and gives incident radiation of known intensity. The brightness of this standard has been calibrated using a tungsten lamp as the primary standard.

Intensity measurement of the oxygen green line, λ5577, in the night airglow emission is the most important undertaking in the night sky division of I. G. Y. researches. In many observatories, engaged in this green line measurement, so called two color photometers are in use, with which the radiation from night sky is measured at two wavelengths, namely at 5577 Å and at 5300 Å, and the contributions of the extra-terrestrial components, star light and zodiacal light, are eliminated by simply taking the difference in deflection for these two wavelengths.

Photometers for the airglow are ordinarily calibrated for absolute intensities from star deflections. In this case, however, there are some inevitable sources to err the outcome, for example, the estimation of effective solid angle of the field of view of the photometer, corrections for the atmospheric extinction, inhomogenity of sensitivity of the photocathode, etc.

For the calibration of absolute sensitivity of the airglow photometers, use of a uniform surface of known brightness seems to give the result more conveniently and accurately than the use of star deflection. For such a type of standard, fulfilment of the following two conditions is desirable: (1) the absolute brightness is given as a function of wavelength, (2) spectral distribution of the emission is close to that of the sun, or has the color temperature of 6000°K.

A brightness standard of this type was constructed to standarise internationally and in Japan the sensitivity of airglow photometers. The construction of the standard is shown in Fig. 1. The light source is a midget tungsten lamp which has the color temperature of 1900°K when lighted at 177.3 ma. d. c. A color glass filter converts the light to that of the color temperature at 6000°K which illuminates an opal glass plate, the surface of which serving as the dummy sky of uniform brightness when the standard is properly mounted on the airglow photometer.

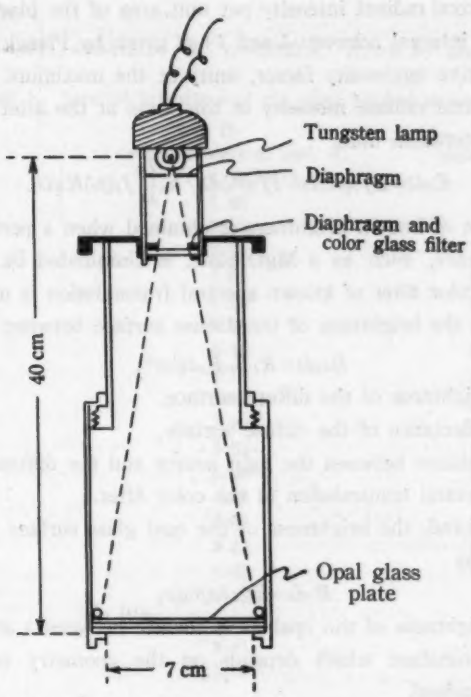

Fig. 1. The brightness standard for the oxygen green line in the night airglow.

The absolute brightness of the opal glass surface was determined by the following procedures. A tungsten filament lamp of known luminosity and of known color temperature was used as the primary standard. The luminosity was 2.85 cd. and the color temperature was 2000°K at 583 ma. dc. of current. These values were determined by Dr. M. Nonaka of the Electrotechnical Laboratory, Tokyo.

Luminous intensity of a tungsten filament lamp of color temperature θ_0 °K is safely given by

$$I = C\, k_m \int_0^\infty J_\lambda(\theta_0) K_\lambda d_\lambda ,$$

where I: luminosity of the lamp in cd. unit,

C: a constant which depends on shape and dimensions of the light source,

k_m: conversion factor from radiant energy to luminosity (=680 lumens/watt),

$J_\lambda(\theta_0)d\lambda$: spectral radiant intensity per unit area of the black body at θ_0°K at the interval between λ and $\lambda+d\lambda$ given by Planck equation,

K_λ: relative luminosity factor, unity at the maximum point.

Then the spectral radiant intensity of this lamp at the interval between λ and $\lambda+d\lambda$ is, in watt/steradian unit,

$$E_\lambda d\lambda = CJ_\lambda(\theta_0)d\lambda = IJ_\lambda(\theta_0)d\lambda \Big/ k_m\int_0^\infty J_\lambda(\theta_0)K_\lambda d\lambda .$$

Thus a surface of known brightness is obtained when a perfect diffuse surface of known reflectance, such as a MgO plate, is illuminated by a lamp of known luminosity. If a color filter of known spectral transmission is used to change the color temperature, the brightness of the diffuse surface between λ and $\lambda+d\lambda$ is

$$B_{0\lambda}d\lambda = R_\lambda T_{0\lambda}E_\lambda d\lambda/\pi r^2 ,$$

where $B_{0\lambda}d\lambda$: brightness of the diffuse surface,

R_λ: reflectance of the diffuse surface,

r: distance between the light source and the diffuse surface,

$T_{0\lambda}$: spectral transmission of the color filter.

On the other hand, the brightness of the opal glass surface of the brightness standard is given as

$$B_\lambda d\lambda = kT_\lambda J_\lambda(\theta)d\lambda ,$$

where $B_\lambda d\lambda$: brightness of the opal glass surface between λ and $\lambda+d\lambda$,

k: a constant which depends on the geometry of the brightness standard,

T_λ: spectral transmission of the color temperature conversion filter used in the brightness standard,

$J_\lambda(\theta)d\lambda$: spectral radiant energy,

θ: color temperature of the light source used in the brightness standard.

Converted color temperature is chosen to be the same for the diffuse surface (MgO plate) and for the opal glass surface. The brightness of these two surfaces is compared by a photometer which is sensitive only in a narrow spectral range centered at λ_1. If the deflections of the photometer are D_0 and D by the diffuse surface (MgO plate) and the opal glass surface, respectively, the brightness of the opal glass between λ_1 and $\lambda_1+d\lambda$ is given as

$$B_{\lambda_1}d\lambda = \frac{DB_{0\lambda_1}d\lambda}{D_0} = \frac{R_{\lambda_1}DT_{0\lambda_1}J_{\lambda_1}(\theta_0)Id\lambda}{\pi r^2 D_0 k_m\int_0^\infty J_\lambda(\theta_0)K_\lambda d\lambda} ,$$

and that between λ and $\lambda+d\lambda$ is

$$B_\lambda d\lambda = \frac{T_\lambda J_\lambda(\theta)B_{\lambda_1}d\lambda}{T_{\lambda_1}J_{\lambda_1}(\theta)} ,$$

for any wavelength, λ.

The standard was calibrated at $\lambda_1=5300$ Å, $R_\lambda=0.96$ and $r=770$ cm, and

Table 1. Spectral brightness of the night airglow standard.

λ mμ	B_λ ergs/sec sterard. cm². Å.	B_λ rayleighs/Å
450	1.39×10^{-6}	3.95
460	1.85	5.35
470	2.35	6.95
480	2.99	8.90
490	3.61	11.10
500	4.22	13.35
510	4.90	15.70
520	5.46	18.00
530	5.77	19.40
540	5.88	20.00
550	5.82	20.10
560	5.53	19.70
570	5.06	18.40
580	4.53	16.50
590	3.88	14.40
600	3.23	12.20
610	2.67	10.10
620	2.12	8.30
630	1.74	6.85
640	1.41	5.85
650	1.26	5.20

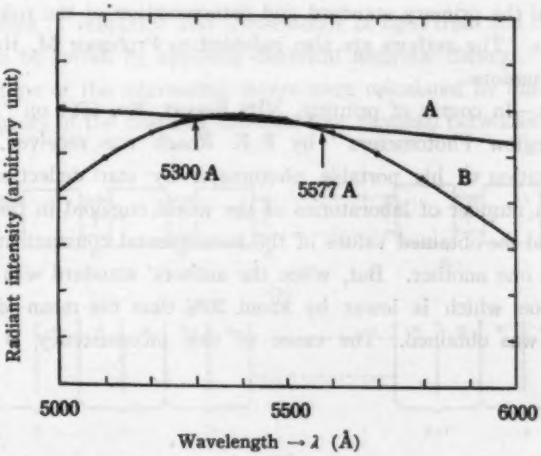

Fig. 2. Spectral distribution of the black body radiation of 6000° K and of the brightness standard.
A: The black body radiation of 6000° K,
B: The brightness standard.

the absolute brightness of the standard determined is shown in Table 1. The brightness given in Rayleigh unit is easily converted from energy unit by multiplying $4\pi/10^6\ h\nu$, (where $h\nu$ is the energy of a photon) and the results are also shown in the same table.

The absolute intensity of the night airglow or the extra-terrestrial components can be determined from comparison of deflections of a photometer for the night sky and for the standard, if the effective band width of the overall spectral sensitivity curve of the photometer is given. It should be noted, however, that the effective band width for the oxygen green line must be determined from the sensitivity curve made unity at 5577 Å.

Though color correction of the light source of the standard by the color glass filters was not perfect, as shown in Fig. 2, the ratio of the radiant intensities at 5300 Å and at 5577 Å was adjusted to be the same as that of the sun, whose color temperature was assumed to be 6000°K, and therefore the equality of the contributions of the extra-terrestrial components at 5300 Å and at 5577 Å in the airglow photometer deflections can be easily examined by this standard.

This brightness standard is now being served to calibrate the airglow photometers in Japan. The absolute intensity of the airglow emissions determined by this standard has been proved to give a fairly good agreement with that determined from star deflections.

The authors would like to thank Dr. Mamoru Nonaka for his kind cooperation in calibration of the primary standard and determination of the color temperatures of many lamps. The authors are also indebted to Professor M. Huruhata for his invaluable discussions.

Addendum.—In course of printing, NBS Report, No. 5591 on "The Intercalibration of Airglow Photometers" by F. E. Roach was received. He gives the result of calibration of his portable photometer by star deflection. Calibration was made at a number of laboratories of the world engaged in the night airglow observation, and the obtained values of the instrumental constant are more or less in accord with one another. But, when the authors' standard was used for calibration, a value which is lower by about 20% than the mean of the values by star deflection was obtained. The cause of this inconsistency is unaccountable as yet.

Reflectivity Curves by Multiple Layers of Alternating Refractive Indices on Image Basis and Lippmann Photography

M. IWATA, S. KATSUBE and T. FUKUDA

Osaka Industrial Research Institute

(Received July 12, 1958)

Abstract

Reflectivity curves by one type of multiple layers of alternating refractive indices were reported formerly[1]. Calculation of the curves was performed by comparing the multiple layers to a chain of four terminal electrical networks connected in the same direction.

In this report another type of multiple layers of alternating refractive indices is discussed. The former type is called "alternating layers on iterative basis" and the latter "alternating layers on image basis". Construction of the layers of these two types and the corresponding circuits are shown schematically.

Optically, the latter type resembles the former type in many respects, but a remarkable difference is found in the shape of reflectivity curves: the curve by the former is symmetric, while that by the latter is asymmetric. It is also found that the reflectivity curve of Lippmann photograph has the same feature as that of alternating layers on image basis.

1. Introduction

The problems of reflection and transmission of light from and through multiple thin layers can be solved by applying electrical network theory. The characteristics of one type of the alternating layers were calculated by one of the authors applying the theory of the chain of identical four terminal networks. Another type

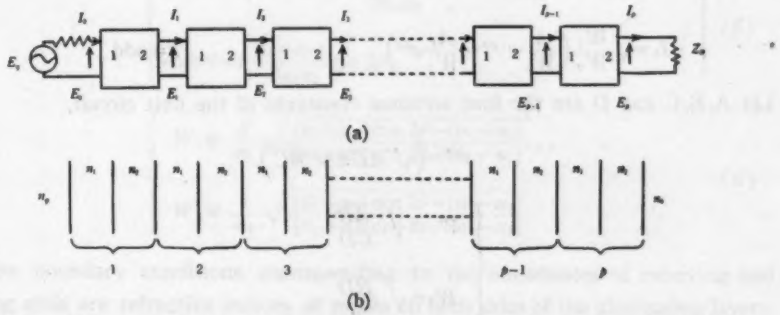

Fig. 1. Alternating Layers on iterative basis (b) and the corresponding circuit (a).

1) M. Iwata: Science of Light **2** 116 (1953).

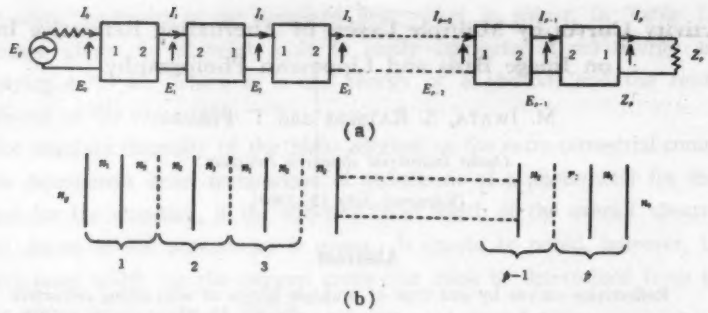

Fig. 2. Alternating layers on image basis (b) and the corresponding circuit (a).

of the alternating layers is considered in this report. Constructions of the layers of these two types and the corresponding electrical circuits are shown in Fig. 1 and Fig. 2. The types shown in Fig. 1 and Fig. 2 are called "the alternating layers on iterative basis" and "the alternating layers on image basis" respectively. Discussion on the reflectivity curves by the former type is given in the previous report. Study of the latter type is the object of this report.

2. Theory of the Chain of Identical Four Terminal Networks on Image Basis[2]

The voltage E_k and the current I_k of k-th terminals of the circuit shown in Fig. 2 (a) are given by the following equations

$$\begin{cases} E_k = A_1 e^{-k\theta} + A_2 e^{k\theta}, & k=\text{even} \\ E_k = \sqrt{\dfrac{W_2}{W_1}}(A_1 e^{-k\theta} + A_2 e^{k\theta}), & k=\text{odd} \\ I_k = \dfrac{A_1}{W_1} e^{-k\theta} - \dfrac{A_2}{W_1} e^{k\theta}, & k=\text{even} \\ I_k = \sqrt{\dfrac{W_1}{W_2}}\left(\dfrac{A_1}{W_1} e^{-k\theta} - \dfrac{A_2}{W_1} e^{k\theta}\right). & k=\text{odd} \end{cases} \tag{1}$$

Let A, B, C and D are the four terminal constants of the unit circuit,

$$e^{\pm\theta} = \left(\sqrt{AD} \pm \sqrt{BC}\right), \tag{2}$$

$$\begin{cases} W_1 = \sqrt{\dfrac{AB}{CD}}, \\ W_2 = \sqrt{\dfrac{BD}{AC}}. \end{cases} \tag{3}$$

2) E. A. Guillemin: "Communication Networks" Vol. II (John Wiley and Sons, 1935) pp 161~166.

The two constants A_1 and A_2 are defined by boundary conditions, i.e. the impedances of the generator and the load.

3. Application of Electrical Network Theory to the Alternating Layers on Image Basis

Network theory described in §2 can be applied to the calculation of reflection and transmission of the alternating layers on image basis. The process is the same as used in the previous report.

Put

$$\delta=\frac{2\pi}{\lambda}n_1d_1=\frac{2\pi}{\lambda}n_2d_2\,,$$

where n_1, d_1 and n_2, d_2 are the refractive index and thickness of the first and second layers respectively, and λ is the wavelength of light in vacuum. Four terminal contants of the layers are given as follows[3],

$$\begin{cases} A=\cos^2\delta-\dfrac{n_2}{n_1}\sin^2\delta\,, \\ B=i\left(\dfrac{1}{n_1}+\dfrac{1}{n_2}\right)\sin\delta\cos\delta\,, \\ C=i(n_1+n_2)\sin\delta\cos\delta\,, \\ D=\cos^2\delta-\dfrac{n_1}{n_2}\sin^2\delta\,. \end{cases} \tag{4}$$

Propagation function θ and image impedances W_1 and W_2 are found from the following equations.

$$\begin{cases} \cosh\theta=\sqrt{\dfrac{(n_1-n_2)^2-(n_1+n_2)^2\cos^2\delta}{2n_1n_2}}\,, \\ \sinh\theta=i\dfrac{n_1+n_2}{\sqrt{2n_1n_2}}\sin 2\delta\,, \end{cases} \tag{5}$$

$$\begin{cases} W_1=\dfrac{1}{n_1}\sqrt{\dfrac{(n_1+n_2)\cos 2\delta+(n_1-n_2)}{(n_1+n_2)\cos 2\delta-(n_1-n_2)}}\,, \\ W_2=\dfrac{1}{n_2}\sqrt{\dfrac{(n_1+n_2)\cos 2\delta-(n_1-n_2)}{(n_1+n_2)\cos 2\delta+(n_1-n_2)}}\,. \end{cases} \tag{6}$$

The boundary conditions corresponding to the impedances of receiving and sending ends are refractive indices of media on both sides of the alternating layers.

Under these conditions reflectivities of p layers are calculated as follows;

3) R. B. Muchmore: J. O. S. A. **38** 954 (1948).

$$\begin{cases} R_{p\text{-odd}} = \left| \dfrac{(n_g n_0 W_1 W_2 - 1)\sinh p\theta + (n_g W_2 - n_0 W_1)\cosh p\theta}{(n_g n_0 W_1 W_2 + 1)\sinh p\theta + (n_g W_2 + n_0 W_1)\cosh p\theta} \right|^2 \\ R_{p\text{-even}} = \left| \dfrac{(n_g n_0 W_1^2 - 1)\sinh p\theta + (n_g - n_0)\cosh p\theta}{(n_g n_0 W_1^2 + 1)\sinh p\theta + (n_g + n_0)\cosh p\theta} \right|^2 . \end{cases} \tag{7}$$

4. Reflectivity Curves

To examine reflectivity curves, the variation must be known of the image propagation function θ, which is generally a complex number. Putting $n_1=1.53$ and $n_2=1.61$ (these values are preferred for convenience to compare the result with the reflectivity curves of Lippmann photographs.) the variation $\theta=\theta_1+i\theta_2$ is shown in Fig. 3. In the regions $\left|\cos\delta\right| > \left|\dfrac{n_1-n_2}{n_1+n_2}\right|$, θ is complex and in other regions θ is purely imaginary. The former are the "attenuation regions" and the latter are the "transmission regions".

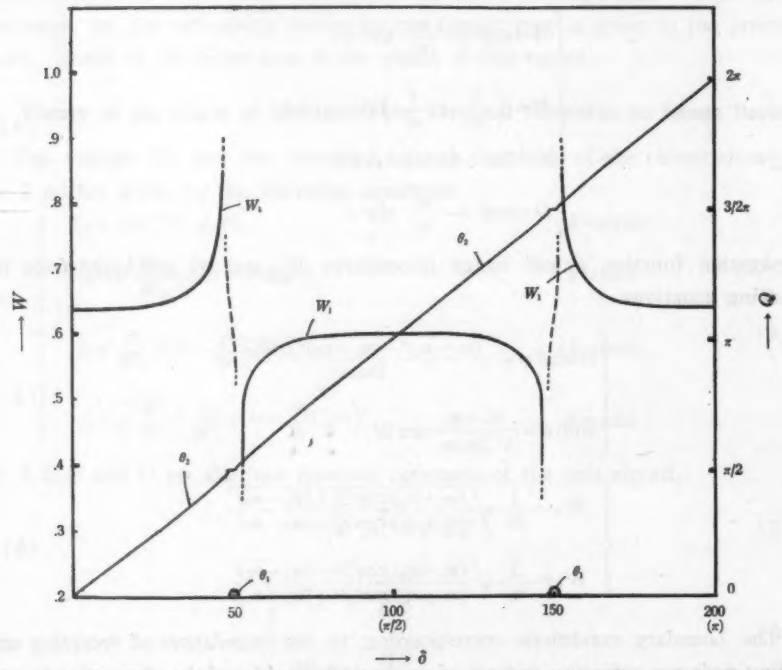

Fig. 3. Propagation function θ and image impedance W_1 according to Eqs. (5) and (6) respectively, in which $n_1=1.53$ and $n_2=1.61$.

The variation of W_1 with δ for the same n_1 and n_2 as above is shown in Fig.

3. W_1 is real in the transmission regions and is imaginary in the attenuation regions. W_2 is deduced easily from W_1 by the relation

$$W_2=\frac{1}{n_1 n_2}\frac{1}{W_1}. \tag{8}$$

Reflectivity curve calculated by Eq. (7) is shown in Fig. 4, in which $n_0=1.0$, $n_1=1.53$, $n_2=1.61$, $n_g=1.53$ and $p=8$ are taken.

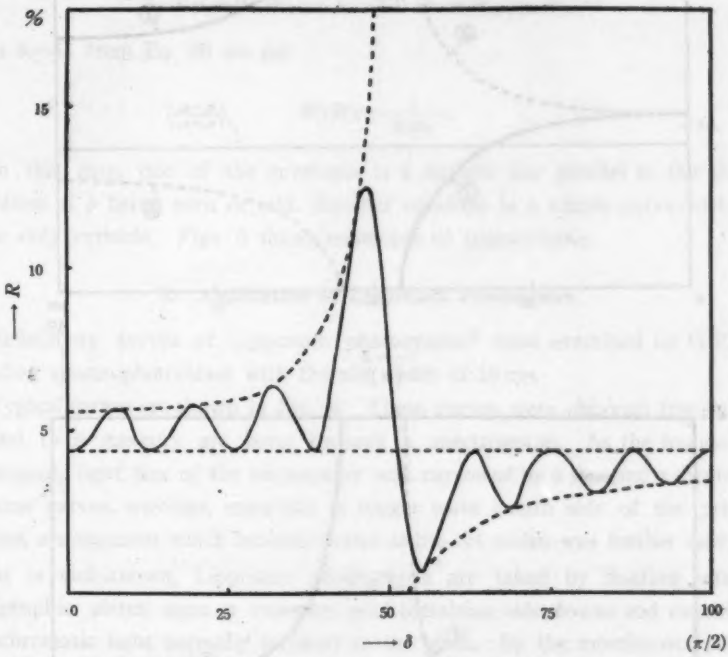

Fig. 4. Reflectivity curve according to Eq. (7), in which $n_0=1.0$, $n_g=1.53$, $n_1=1.53$, $n_2=1.61$ and $p=8$.

Comparison of the reflectivity curve of the alternating layers on image basis with that of the alternating layers on iterative basis is as follows:

The quality common to both is that in transmission regions the curve fluctuates and has low values and in attenuation regions it attains a very high value (principal maximum). But in the image type the curve is asymmetric and in the iterative type symmetric with reference to the vertical line through the principal maximum.

Envelope ϕ of reflectivity curves for various numbers of layers p, can be found by putting

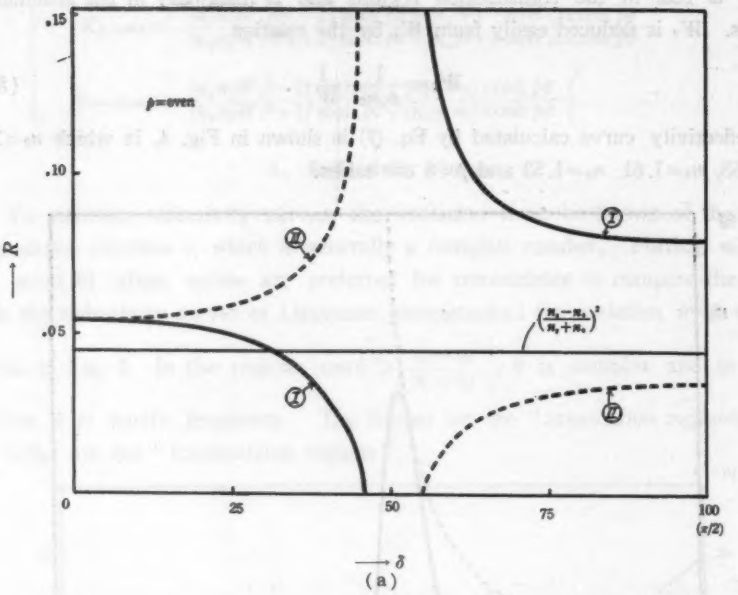

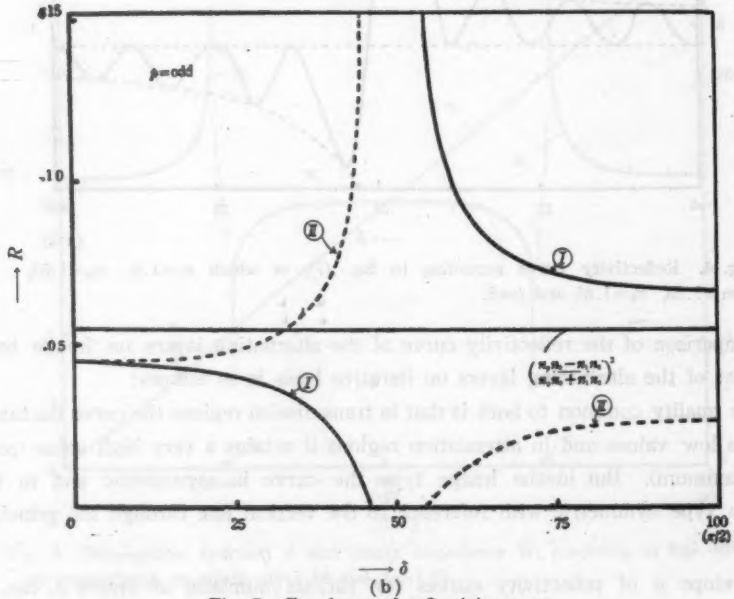

Fig. 5. Envelopes of reflectivity curve:
① $n_1=1.61$ $n_2=1.53$ ② $n_1=1.53$ $n_2=1.61$

$$\frac{\partial R}{\partial p}=0, \tag{9}$$

and eliminating p from (8) and (9),

$$\begin{aligned}\phi_{\text{even}}&=\left(\frac{n_g-n_0}{n_g+n_0}\right)^2 \quad \text{and} \quad \left(\frac{n_g n_0 W_1{}^2-1}{n_g n_0 W_1{}^2+1}\right)^2,\\ \phi_{\text{odd}}&=\left(\frac{n_g n_1 W_1 W_2-1}{n_g n_0 W_1 W_2+1}\right)^2 \quad \text{and} \quad \left(\frac{n_g W_2+n_0 W_1}{n_g W_2+n_0 W_1}\right)^2.\end{aligned} \tag{10}$$

When $\delta_1=\delta_2$, from Eq. (6) we get

$$W_1 W_2=\frac{1}{n_1 n_2}.$$

In this case, one of the envelopes is a straight line parallel to the abscissa regardless of p being even or odd. Another envelope is a simple curve with $\tan^2\delta$ as the only variable. Figs. 5 shows envelopes of typical cases.

5. Application of Lippmann Photograph

Reflectivity curves of Lippmann photographs* were examined by G.E. self-recording spectrophotometer with the slit width of 10 mμ.

Typical curves are shown in Fig. 6. These curves were obtained from a plate exposed to a mercury arc lamp through a spectrograph. As the images were line shaped, light flux of the photometer was narrowed by a lens and a diaphragm. On these curves, wavings, especially in longer wave length side of the principal maxima, are apparent which became clearer as the slit width was further narrowed.

As is well-known, Lippmann photographs are taken by floating ultra-fine photographic plates upon a mercury pool (emulsion side down) and exposing to monochromatic light normally incident to the plate. By the interference between incident rays and reflected rays from mercury surface, stationary waves are set up.

Emulsion grains near the loops of the stationary waves form latent images and grains near the node remain unaffected. After developing, there appear alternating layers containing silver grains and no silver grains. The optical thickness of each layer is a quarter of wave length of the incident light. In the present experiment, plates were bleached by mercuric chloride solution after fixing. The silver grains seemed to be changed to silver chloride grains. As silver chloride has a high refractive index, the layers containing silver chloride grains must have a higher index than the layers containing no silver chloride. Hence Lippmann

* These photographs were taken by Prof. H. Kubota of Tokyo Univ. and Mr. T. Yasuno of Oriental Developing Lab. of Agfa Photo Industry.

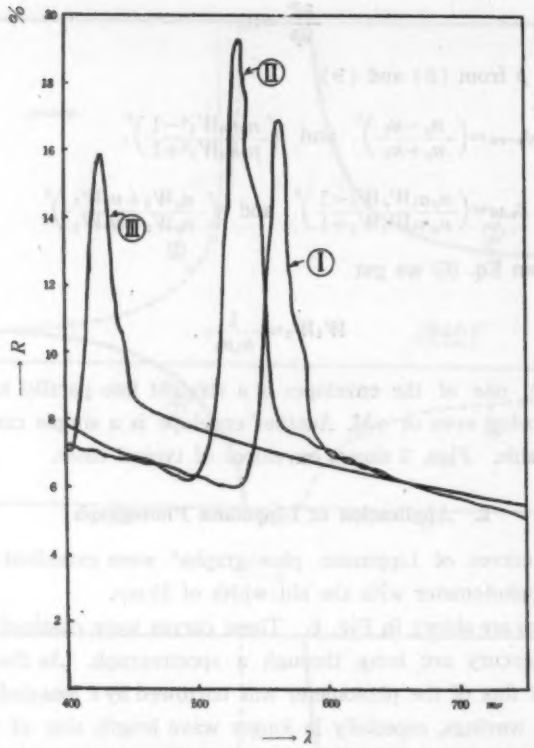

Fig. 6. Spectrophotometric curves of a Lippmann photograph exposed to a mercury arc lamp Ⅰ 5770–90 lines Ⅱ 5461 line Ⅲ 4358 line

photograph can be regarded as multiple layers of alternating high and low refractive indices, the optical thickness of each layer being nearly a quarter of wave length of the exposed light.

Since mercury can be assumed here as an ideal conductor, the stationary wave must have a node at its surface. Fig. 7. shows schematically the stationary waves and the developed multiple layers at the surface of the plate. We can see from

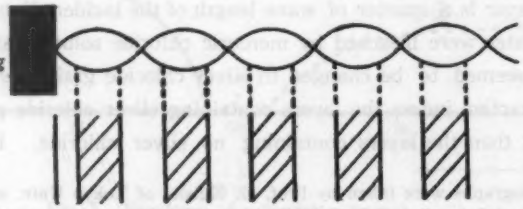

Fig. 7. Stationary waves and developed multiple layers at the surface of the plate.

this figure that Lippmann plate has the very construction of the alternating layers on image basis.

Comparison of the reflectivity curve of Lippmann plate (Fig. 6) to that of the alternating layers on image basis (Fig. 3) confirms the above argumentation being adequate. Dispersion of optical constants, especially that of silver chloride, can explain the disagreement that reflectivity of Lipmann plate is higher in the shorter wave-length region than that of alternating layers.

Delcroix[4] reported measurements made on reflectivity curves of Lippmann photographs. His results agree very well with the authors'.

Acknowledgment

The authors express gratitude to Prof. H. Kubota of Tokyo Univ. and Mr. T. Yasuno for their kind offer of Lippmann plates.

4) J. L. Delcroix: Revue d'Optique **27** 493 (1948).

Current Dependence of Decay of Metastable Mercury Atoms in Argon-Mercury Discharge Afterglows

Masahiro YOKOYAMA

Institute of Physics, North College, Osaka University

(Received April 28, 1958)

Abstract

The decay of $6^3P_{2,0}$ metastable states of mercury have been studied by the optical absorption method in the afterglow of argon-mercury discharge at 300°K. Measurements show that lifetimes of $6^3P_{2,0}$ mercury metastable states are dependent upon the amplitude of excitation pulse used to create the metastables in the absorption tube.

1. Introduction

Experimental studies on metastable rare gas and mercury atoms, for which the optical transition through emission of electric dipole radiation from metastable state is forbidden by the selection rule, have been made by many investigators[1].

These experiments were based on the principle that the density of metastable atoms in the afterglow of an interrupted discharge can be measured by the optical absorption observed at appropriate wavelengths.

After World War II, progress in experimental techniques, especially the development of pulse techniques and employment of photomultiplier as a light detector[2], pressed forward the investigation in this field.

Results of experiment made on the time transients of optical absorption for metastable mercury atoms in the afterglow of argon-mercury discharge are presented below.

2. Theory for Absorption Studies[3]

If a parallel light beam of intensity I_0 and frequency ν from emission tube be sent through an absorbing layer containing a gas, the intensity I of the transmitted light at frequency ν is given by

1) H. S. W. Massey and E. H. S. Burhop: Electronic and Ionic Impact Phenomena, (Oxford University Press, London, 1953).
2) R. W. Engstrom: Jour. Opt. Soc. Am. **37** (1947) 420.
3) A. C. G. Mitchell and M. W. Zemansky: Resonance Radiation and Excited Atoms (University Press, Cambridge, 1934).

$$I=I_0e^{-k_\nu l} \tag{1}$$

where l is the thickness of the absorbing layer and k_ν is the absorption coefficient of the gas.

It is well known that, if natural damping is neglected and only the heat motions are taken into account, the absorption coefficient of a gas is given by

$$k_\nu=k_0e^{-\omega^2}. \tag{2}$$

Here
$$\omega=\frac{2(\nu-\nu_0)}{\Delta\nu_0}\sqrt{ln2}. \tag{3}$$

and $\Delta\nu_0$ is the Doppler breadth and ν_0 is the frequency of the center of absorption line. The quantity k_0 is the maximum absorption coefficient when Doppler broadening alone is present and is given by

$$k_0=\frac{2}{\Delta\nu_0}\sqrt{\frac{ln2}{\pi}}\frac{\lambda^2_0g_n}{8\pi g_m}A_{nm}M_m \tag{4}$$

where λ_0 is the wavelength corresponding to frequency ν_0, g_m and g_n are the respective statistical weights of states m and n, A_{nm} is the Einstein coefficient for the spontaneous transition from state n to state m and M_m is the number of atoms in state m per. cm^3.

The absorption A is defined by

$$A=1-\frac{I}{I_0}. \tag{5}$$

It is often necessary to use an empirical expression for the frequency distribution of the emitted radiation from emission tube in which either the vapor pressure or the thickness of the emitting layer or both are not accurately known. A conventional expression for the emission line frequency dependence is given by

$$I_\nu=I_{\nu_0}e^{-(\omega/\alpha)^2} \tag{6}$$

where I_{ν_0} is the center intensity

and
$$\alpha=\frac{\text{emission line breadth}}{\text{absorption line breadth}}. \tag{7}$$

Now, the light beam intensity I_0 is represented by

$$I_0=\int I_\nu d\nu. \tag{8}$$

Then, Equation (5) is reduced to the form of[4]

$$A_a=\frac{k_0l}{\sqrt{1+\alpha^2}}-\frac{(k_0l)^2}{2!\sqrt{1+2\alpha^2}}+\cdots\cdots-(-1)^n\frac{(k_0l)^n}{n!\sqrt{1+n\alpha^2}}+\cdots\cdots \tag{9}$$

Under usual experimental conditions, except in a small time interval after the removal of excitation, the concentration of metastable atoms decays exponentially

4) M. W. Zemansky: Phys. Rev. **36** (1930) 219.

with time. Thus,

$$M_m = M_{m_0} e^{-t/\tau} \tag{10}$$

when M_m is the average number of metastable atoms per cm^3 in the absorbing layer. M_{m_0} is the concentration of metastable atoms at the initial stage of decay after the excitation is over and τ is the lifetime of metastable atoms concerned.

Therefore, if α is small, Equation (9) may be written in the following form using Equations (4) and (10),

$$\ln k_0 l = -\frac{t}{\tau} + \text{constant}. \tag{11}$$

Thus, the lifetime τ of metastable state is obtained by measuring the absorption A as a function of time in the afterglow of the discharge after the excitation has ceased.

3. Experimental Procedure

Principle of the present experiment is based upon measuring the optical absorption caused by the mercury metastable atoms as a function of time in the afterglow of argon-mercury discharge with apparatus essentially similar to those used by F. A. Grant[5] et al.[6]

Schematic diagram of the experimental arrangement is shown in Fig. 1.

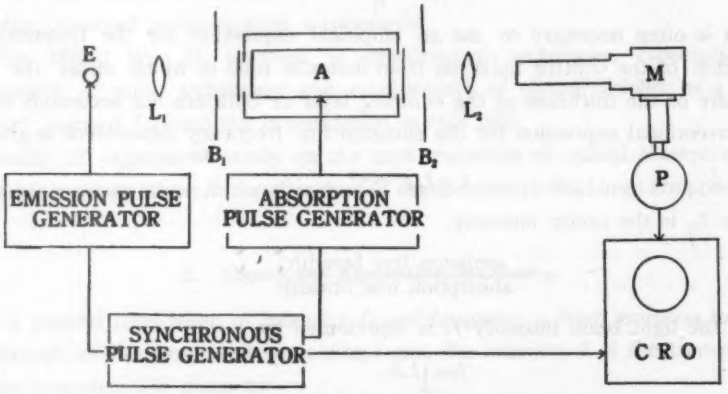

Fig. 1. Schematic diagram of experimental apparatus.
E: Emission tube, A: Absorption tube,
L_1, L_2: Lenses, B_1, B_2: Baffles,
M: Monochromator, P: Photomultiplier,
CRO: Cathode-ray oscilloscope.

5) F. A. Grant: Can. Jour. Res. **A28** (1950) 339.
6) F. A. Grant and A. D. Krumbein: Phys. Rev. **90** (1953) 59.

Visible light of mercury from emission tube E is passed through a monochromator M after travelling the absorption tube A, which contains the gas to be studied. Monochromatic light is incident on the photomultiplier P and its amplified voltage output is displayed on the screen of cathode-ray oscilloscope. Emission tube E is excited with about 1000–3000 c.p.s. pulse repetition frequency by an emission pulse generator, while the absorption tube A is excited with 100–400 c.p.s. by an absorption pulse generator.

The procedure of measuring the optical absorption as a function of time is shown in Fig. 2. In this figure, (A) is the waveform of the monochromatic light pulse from the absorption tube A excited by the absorption pulse generator and the concentration of atoms excited to the metastable state in the absorption tube may be shown by (B). Waveform of the same monochromatic light pulse from the emission tube E is also illustrated by (C). Then, (D) is the final oscilloscope pattern caused by the absorption of metastable atoms, which is a measure of the concentration of metastable atoms in the decay period such as shown in (B).

The lifetimes of metastable atoms corresponding to the wavelength of absorbed light beam from the emission tube are thus determined by measuring the absorption in decay period on photographs of the cathode-ray tube screen.

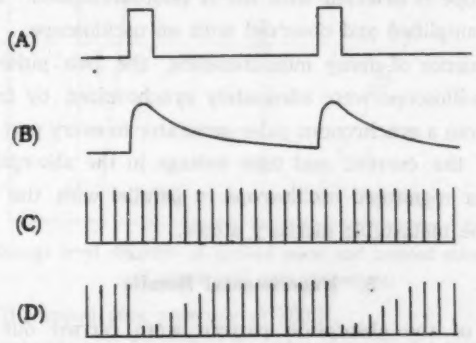

Fig. 2. Procedures of detecting the decay of the absorption patterns of metastable atoms.

4. Experimental Apparatus

The absorption tube A is of cylindrical hard glass and is circular in cross-section with flat window and ring electrode at both ends. The electrodes are circular rings made of tungsten wire of 0.4 mm or 0.9 mm in diameter and arranged concentric with the walls of the absorption tube of 6 cm in inside diameter and 30 cm in length. The absorption tube was baked at 450°C while being evacuated

for 15 hours with the tungsten electrodes heated to incandescence, then argon gas and one drop of mercury were introduced into it and sealed off. The argon gas had been purified by magnesium getter and the mercury carefully distilled three times in vacuum to ensure its purity. Repeated discharge was found very effective in removing impurities in the absorption tube.

The emission tube is a cold cathode capillary discharge tube of 2 mm in inside diameter and 5 cm in length filled with argon-mercury gas mixture. The capillary source emits the emission line determined by the Doppler effect alone, uninfluenced by self-reversal of the emission line. It was important to avoid fluctuations of the amplitude of light pulse from the emission tube, which affect seriously the accuracy of observation.

Both emission and absorption pulse generators consisting of so-called multivibrator were designed to produce square wave pulses of 1000–3000 c.p.s. and 100–400 c.p.s. respectively. The frequency and duration of these excitation pulses are made adjustable. The use of pulse excitation in emission and absorption tubes reduces the temperature rise in both tubes to a negligible value enabling all forms of broadening of the emission and absorption lines to be kept minimum.

The visible light pulse of mercury spectral lines separated by a constant deviation spectroscope is detected with 931-A photomultiplier. The output of the photomultiplier is amplified and observed with an oscilloscope.

For the convenience of decay measurements, the two pulse generators and the cathode-ray oscilloscope were adequately synchronized by transmitting audio frequency signals from a synchronous pulse generator to every part of the apparatus.

Waveforms of the current and tube voltage in the absorption tube are also observed by another monitored oscilloscope in parallel with the measurement of decay pattern of the metastable mercury atoms.

5. Experimental Results

Measurements of the absorption pattern were carried out on three visible triplet lines, λ5461 4358 and 4047 Å lines, of mercury atom. These lines, λ5461, 4358 and 4047 Å, have 7^3S_1 level as a common initial level and end in $6^3P_{2,1,0}$ states respectively as shown in Fig. 3. Here, $6^3P_{2,0}$ states are metastable and 6^3P_1 state is a resonance level.

As expected, λ4047 and 5461 Å lines, which have metastable states as end levels, have shown decay patterns of absorption, while for λ4358 Å line no pattern of absorption has been observed at 300°K. Typical decay pattern of mercury metastable atom is shown in Fig. 4. This photograph is the decay pattern of 6^3P_0 metastable mercury atom obtained from the absorption of λ4047 Å line (6^3P_0—

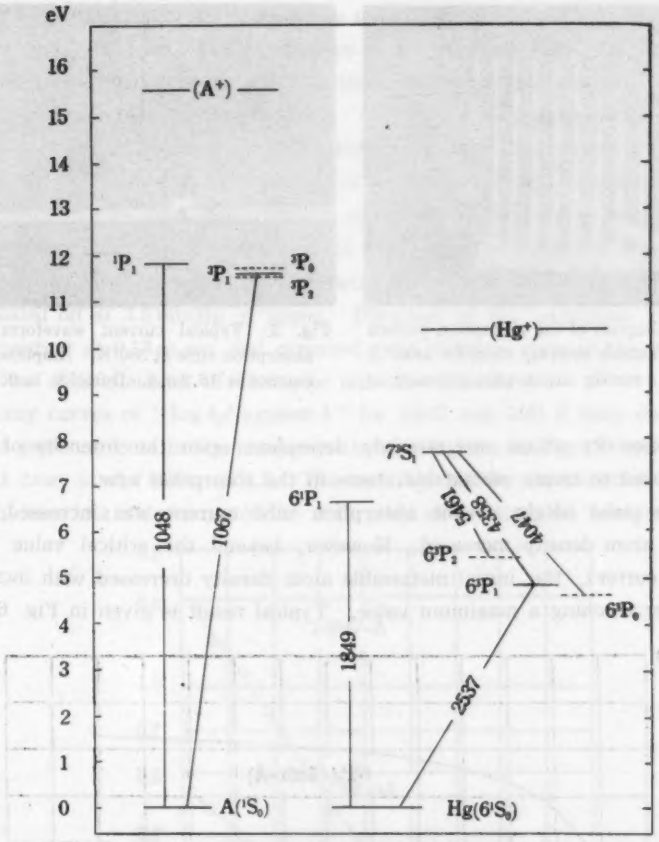

Fig. 3. Energy level diagram of ground state and excited state configurations of argon and mercury atoms.

7^3S_1) at 3.4 mmHg argon plus mercury at 300°K.

In Fig. 5, current waveform is also shown, in which the peak current is 16.2 mA and the current duration is 0.13 m sec.

Since the observed oscilloscope patterns of the current in the absorption tube are of square wave pulse, discharge current in the absorption tube can be changed by varying either the pulse height or the duration of the excitation pulse. In the present experiment, the variation of metastable lifetimes with excitation current was measured mainly by changing the amplitude of the current pulse[7].

Then, it was found that the decay rates of both metastable 6^3P_2 and 6^3P_0

7) A. H. Futch and F. A. Grant: Phys. Rev. **104** (1956) 356.

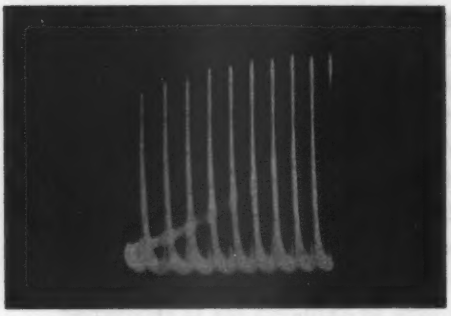

Fig. 4. Oscillogram of the absorption pattern of 6^3P_0 metastable mercury atom for λ4047 Å line at 3.4 mmHg argon plus mercury at 300°K.

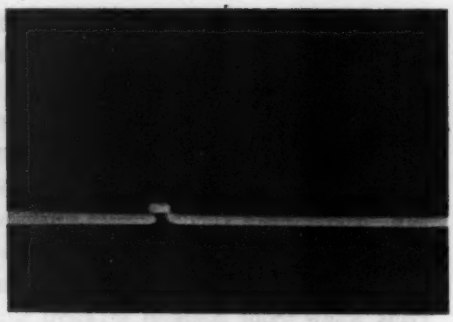

Fig. 5. Typical current waveform in the absorption tube at 300°K. Amplitude of the current is 16.2 mA. Duration is 0.13 msec.

states of mercury atoms are strongly dependent upon the intensity of pulsed discharge used to create metastable atoms in the absorption tube.

As the pulse height of the absorption tube current was increased, initial metastable atom density increased. However, beyond the critical value of the excitation current, the initial metastable atom density decreased with increasing current after reaching a maximum value. Typical result is given in Fig. 6. The

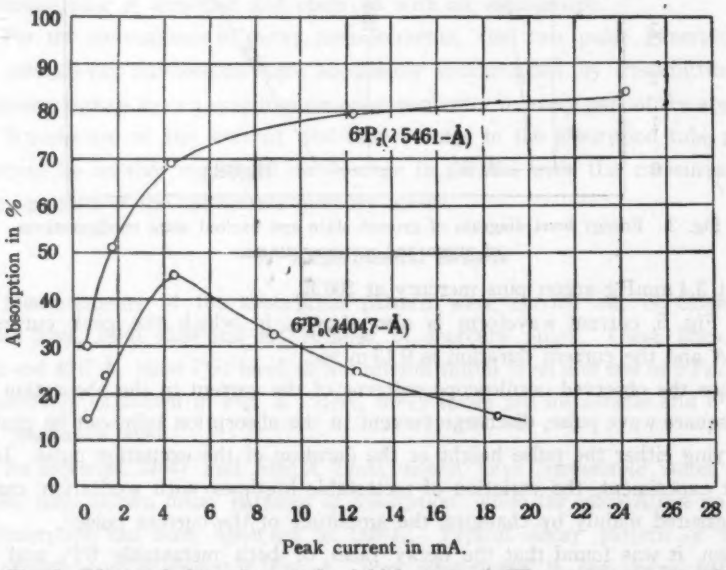

Fig. 6. Measured absorption at the initial stage of $6^3P_{2,0}$ mercury metastable atoms with the peak current of excitation pulse of the absorption tube at 2.2 mmHg argon pressure.

experimental data were taken under the condition of 2.2 mmHg of argon in the absorption tube, when the pulse duration was 0.66 m sec. As the argon pressure in the absorption tube increased, position of the absorption maximum shifted toward the high current density side. In this case, current patterns in the absorption tube tend to have peaks in the ending of pulse duration with increasing argon pressure. These reducing effect of metastable atom density with current seems to be due to the higher electron and ion density in the absorption tube.

In order to investigate the nature of decay of the metastable mercury atom with current, measurements of its lifetime were carried out with an absorption tube sealed off at 3.5 mmHg of argon. Duration of the excitation current was kept constant at 0.13 m sec, and observed peak voltages were in the range of 280–660 volts. The character of discharge was shown positive.

Decay curves of "$\log k_0 l$ against t" for λ4047 and 5461 Å lines observed with various peak currents in the absorption tube are given in Fig. 7 and 8. In the present case, α was taken as 1.5. The fact that all the experimental data fall in straight lines in a wide range of the absorption shows that the fundamental decay

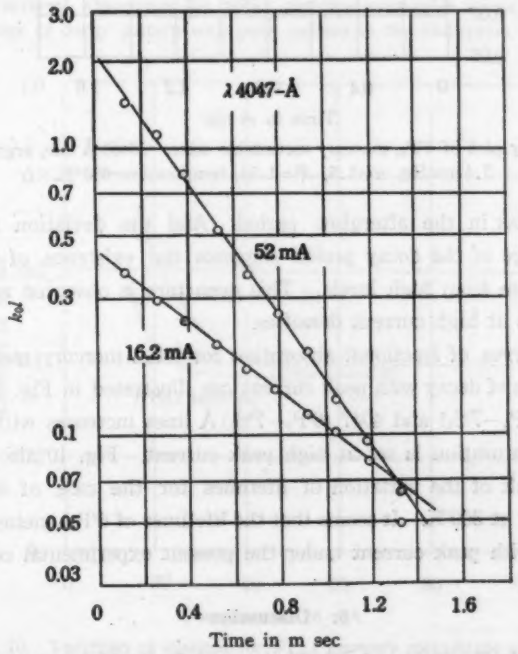

Fig. 7. Decay plots of the 6^3P_0 mercury metastable state illustrating the effect of excitation pulse in the absorption tube. λ4047 Å line, argon pressure 3.4 mmHg, α=1.5, J^2=1.54, temperature 300°K.

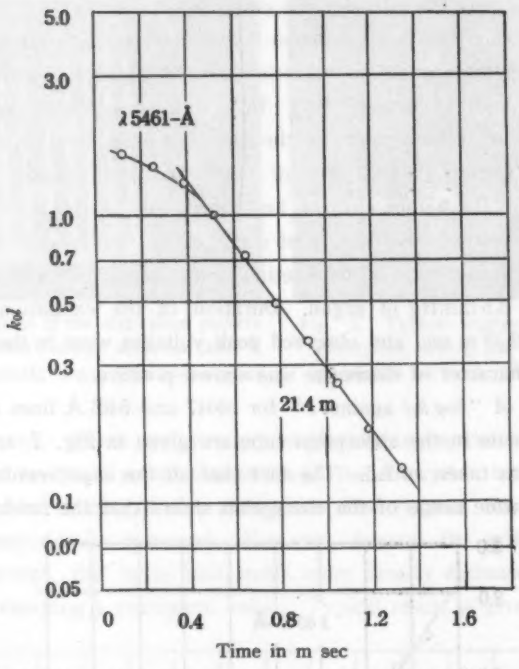

Fig. 8. Decay plot of 6^3P_2, mercury metastable state. λ5461 Å line, argon pressure 3.4 mmHg, $\alpha=1.5$, $I^2=1.54$, temperature 300°K.

mode predominates in the afterglow period. And the deviation from linearity at the initial stage of the decay period suggests the existence of replenishment of metastable state from high levels. This departure is observed mostly on 6^3P_2 metastable atoms at high current densities.

Observed curves of fractional absorption for $6^3P_{2,0}$ mercury metastable atoms at the initial stage of decay with peak current are illustrated in Fig. 9. Absorption of both λ5461 ($6^3P_2-7^3S_1$) and 4047 ($6^3P_0-7^3S_1$) Å lines increases with peak current and substantial saturation is set at high peak current. Fig. 10 also illustrates the experimental result of the variation of lifetimes for the case of $6^3P_{2,0}$ mercury metastable atoms at 300°K. It seems that the lifetimes of $6^3P_{2,0}$ metastable mercury atoms decrease with peak current under the present experimental conditions.

6. Discussion

Recently, F. A. Grant also A. V. Phelps and J. P. Molnar[8] carried out the

8) A. V. Phelps and J. P. Molnar: Phys. Rev. **89** (1953) 1202.

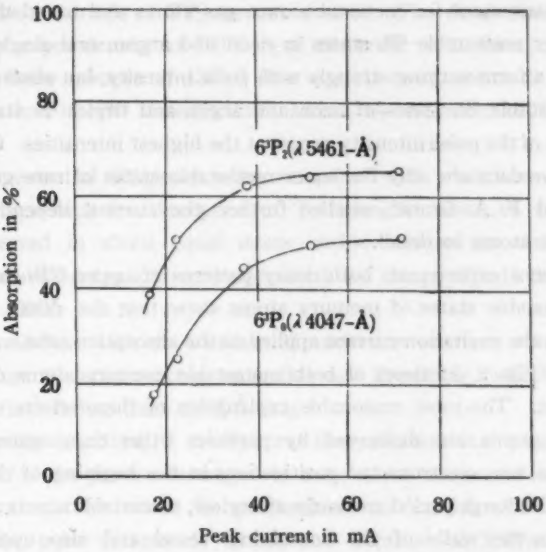

Fig. 9. Fractional absorption for $6^3P_{2,0}$ mercury metastable atoms at the initial stage of decay pattern with peak current in the absorption tube.

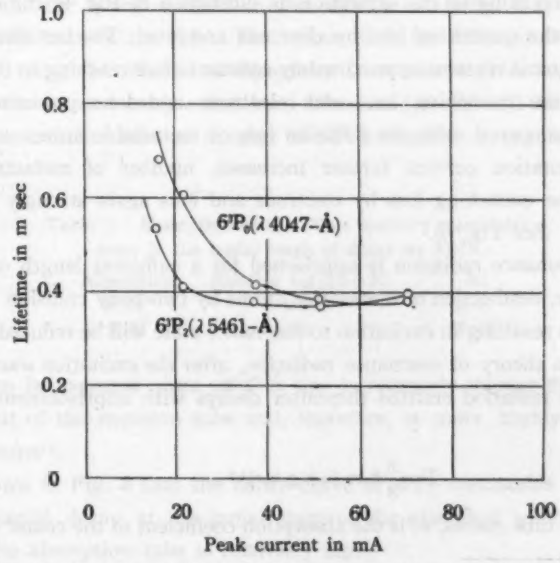

Fig. 10. Variation of lifetime for $6^3P_{2,0}$ mercury metastable atoms at 300°K with excitation current in the absorption tube.

absorption measurement for metastable rare gas atoms and found that absorption curves for upper metastable $^3P_0$ states in neon and argon, and singlet $^1S_0$ state in helium exhibit a form varying strongly with pulse intensity, but absorption patterns for lower metastable $^3P_2$ states of neon and argon and triplet $^3S_1$ state of helium are independent of the pulse intensity except at the highest intensities. Consequently, their quantitative data are only for lower metastable states of rare gases. Lately, J. R. Dixon and F. A. Grant[9] studied further the current dependence of $^3P_{0,2}$ metastable neon atoms in detail.

In the present experiment, both decay patterns of upper 6^3P_2 metastable and lower 6^3P_0 metastable states of mercury atoms show that the decay phenomenon is dependent on the excitation current applied to the absorption tube. As illustrated in the curves of Fig. 8, lifetimes of both metastable mercury atoms decrease with the peak current. The most reasonable explanation of these effects may be that the metastable atoms are destroyed by particles other than neutral atoms and metastable atoms, i. e., electrons and positive ions in the begining of the afterglow.

During the discharge period and early afterglow, metastable atoms are destroyed upon diffusion to the walls of the containing vessel and also upon quenching collision with electrons and ions.

Since the absorption measured at the initial stage of decay increases with current before reaching to the saturation as illustrated in Fig. 9, the diffusion loss is larger than the quenching loss by electrons and ions. The fact that the number of metastable atoms remains approximately constant after reaching to the saturation indicate that the quenching loss with electrons and ions presumably becomes important as compared with the diffusion loss of metastable atoms to the walls. When the excitation current further increases, number of metastable atoms is reduced, for the quenching loss by electrons and ions again strongly exceeds the diffusion loss. (See Fig. 6).

If 2537 resonance radiation is imprisoned for a sufficient length of time in the absorption tube, destruction of metastable atoms by two-body collision with neutral mercury atoms resulting in excitation to resonance state will be reduced. According to the diffusion theory of resonance radiation, after the excitation source is cut-off, 2537 resonance radiation emitted thereafter decays with imprisonment time T as given by[10]

$$T=\frac{5}{8}k_0 r\tau\,(\pi \log k_0 r)^{1/2}$$

where r is the tube radius, k_0 is the absorption coefficient of the center of resonance

9) J. R. Dixon and F. A. Grant: Phys. Rev. **107** (1957) 118.
10) D. Alpert, A. O. McCoubrey and T. Holstein: Phys. Rev. **76** (1949) 1257.

line and τ is the mean life of 6^3P_1 resonance state. The decay time of 6^3P_1 state at the mercury vapor density at 300°K is of the order of 10^{-6} sec. Therefore, the fact that no decay pattern of 4358 Å line was observed, seems to be due to the rapid radiation loss of 6^3P_1 state mercury atoms by emission of 2537 resonance radiation.

This is an essential difference when compared with what was seen in the case of rare gases, in which the absorption of $^3P_1$ resonance state of rare gas atoms could be observed in about equal decay period because the energy separations between metastable states and resonance level are comparable to thermal agitation energy kT at 300°K.

It was found that with the increase of excitation current, the absorption at the initial stage of decay reaches saturation and thereafter λ5461 Å line is always strongly absorbed rather than λ4047 Å line.

As previously described, if the spectral line radiation that passed through the absorbing layer of the gas is unchanged in nature, the number of absorbing atoms in the absorption tube would be proportional to $\log(1/1-A)$. The values of $\log(1/1-A)$ for peak current of 52 mA and duration of 0.13 m sec have been evaluated, and their ratios are given in Table 1.

M. W. Zemansky[4] gives the solution of the problem of obtaining $k_0 l$ from measured A and the ratios of effective line breadth α. Here, k_0 is the absorption coefficient of the core of the line. The values of k_0 for different lines have been calculated by using the relation of Zemansky from measured A and are given in Table 1. In the present case, α has been taken as 1.5. It will be seen that k_0 gives somewhat smaller ralative number of 6^3P_2 metastable state than do the values of $\log(1/1-A)$.

Table 1. Absorption of the $6^3P_{2,0}$ mercury matastable state in the initial stage of decay at 300°K

Line	Absorption	Relative $\log(1/1-A)$	$k_0 l$	Relative k_0
5461	0.64	100	2.61	100
4047	0.49	65	1.46	56

This is to be expected since λ4047 Å line is relatively sharper than λ5461 Å line in coming out of the emission tube and, therefore, is more highly absorbed per absorbing atoms[11].

It is shown in Fig. 8 that the decay curve of 6^3P_2 metastable state deviates from exponential decay at the initial stage of the afterglow when the excitation current in the absorption tube is relatively high.

11) C. Kenty: Jour. App. Phys. **21** (1950) 1309.

A. O. McCoubrey[12] measured the intensity of fluorescent radiation of mercury vapor as a function of time in the afterglow using the time sampling technique. His experimental data illustrate that the decay curve of the measured intensity in the afterglow of Hg_2 fluorescence has an initial relatively slow decay rate, attaining finally a constant slope characteristic of the exponential form. He concluded that 4850 Å band and 3350 Å band had a common persistent reservoir of molecular excitation which feeds both bands. These situations are expressed by the reaction of

$$Hg_2(^3Ou^-) \longrightarrow 2Hg + h\nu(3350),$$

$$Hg_2(^3Ou^-) + 2Hg \longrightarrow 4Hg + h\nu(4850).$$

A. V. Phelps[13] observed the time variation of absorption of helium metastable atoms and molecules. His experimental results show that the decay in the absorption of 5016 Å line by 2^1S_0 metastable helium atoms is accompanied by an increase in the absorption of 3889 Å line by 2^3S_1 metastable helium atoms. This suggests that atoms in 2^1S_0 state are being converted into atoms in 2^3S_1 state by collisions with thermal electrons in early afterglows according to the reaction of

$$He(2^1S_0) + e \longrightarrow He(2^3S_1) + e + 0.79\,eV.$$

In late afterglows, triplet 2^3S_1 metastable atoms are destroyed upon diffusion and also by collisions with two neutral atoms which result in the formation of molecules in $2^3\Sigma_u^+$ state. Time variation curves of absorption for 3889 Å line and 4650 Å band are also interpreted as showing that, as 2^3S_1 metastable atoms are destroyed, there is a rise in the density of $2^3\Sigma_u^+$ metastable molecules in the early afterglows as a result of the reaction,

$$He(2^3S_1) + 2He \longrightarrow He_2(2^3\Sigma_u^+) + He.$$

Thereafter, $2^3\Sigma_u^+$ helium metastable molecules are destroyed upon diffusion to the walls and also by collisions with slow electrons or other metastables.

M. A. Biondi[14] studied the atomic collision process occuring in gases by microwave observation of electron density during the afterglow. He measured the electron density decay in low pressure helium and neon afterglows and confirmed experimentally the hypothesis that the initial increase in electron density is the result of ionization among metastable atoms. Further, he observed the rise and decay of electron density in the afterglow of helium-argon mixtures and concluded that this increase in electron density is the result of metastable-admixed atom collisions[15].

A similar metastable-metastable ionization process is observed in pure mercury

12) A. O. McCoubrey: Phys. Rev. **93** (1954) 1249.
13) A. V. Phelps: Phys. Rev. **99** (1955) 1309.
14) M. A. Biondi: Rev. Sci. Instr. **22** (1951) 500.
15) M. A. Biondi: Phys. Rev. **88** (1952) 660.

afterglows[16] from measured electron density decay curves. In this case, the increase of the electron density in early afterglows is explained by the ionization resulting from collisions between two metastable atoms by the reaction of

$$Hg^* + Hg^* \longrightarrow Hg^+ + Hg + e .$$

In the late afterglows, electrons are lost by ambipolar diffusion to the walls and by collisions with normal mercury atoms.

M. A. Biondi[17,18] also showed previously that the large recombination observed in microwave afterglows requires the presence of molecular ions. This process is evidently dissociative recombination which, in the case of mercury, follows the reaction of

$$Hg_2^+ + e \longrightarrow Hg^* + Hg$$

where * indicates the excited atom.

According to the experiment made by M. A. Biondi[16], the formation of appreciable numbers of mercury molecular ions was observed.

It may be probable that the replenishment process of mercury metastable atoms which occurs in the initial stage of afterglow in the present experiment, be due to the dissociative recombination of electrons with mercury molecular ions formed by the conversion of mercury atomic ions to the molecular ions by three-body collision with neutral argon and mercury atoms by the reaction of

$$Hg^+ + Hg + A \longrightarrow Hg_2^+ + A .$$

To verify these conclusions, further detailed research is necessary. Experiments are being continued.

Acknowledgments

The author wishes to express his hearty thanks to Prof. T. Asada, Institute of Physics, Faculty of Science, Osaka University, for his constant encouragement and kind support during the course of the present experiment. He would also like to express sincere thanks to Prof. M. Shoda, Institute of Physics, North College, Osake University, for his great help and enthusiastic support throughout the entire course of this investigation. Thanks are also due to Prof. K. Honda, Institute of Physics, Faculty of Science, Tokyo University, for his many helpful comments throughout this work. It is also a pleasure to acknowledge the very great contribution made by Mr. Y. Kuroda for carrying out many of the measurements. Lastly, he wishes to express appreciation to Prof. H. Yoshinaga, Department of Applied Physics, Faculty of Engneering, Osaka University, for his taking great interest in this research and its publication.

16) M. A. Biondi: Phys. Rev. **90** (1953) 730.
17) M. A. Biondi and T. Holstein: Phys. Rev. **82** (1951) 962.
18) M. A. Biondi: Phys. Rev. **83** (1951) 1078.

Anomalous Band Features of OH Groups due to Hydrogen Bonding

Yoshiki SATO

Institute for Optical Research, Tokyo University of Education, Shinjuku-ku, Tokyo, Japan

(Received June 7, 1958)

Abstract

Shapes of two absorption bands associated with hydrogen bond formation between phenol and some proton acceptor molecules are examined and shown to be characterized in good approximation by Gaussian distribution function. Factors by which the band shapes are determined are calculated semi-empirically in considerably good agreement with experimental values. As a result, origin of anomalous band features of OH group due to hydrogen bonding is reduced to distribution of the O. .O distance. Further, by making use of the perturbation theory, features of double minimum potential for the motion of proton are analyzed, as in the case of methanol, and the period of time which is spent by the proton jumping from one minimum potential to the other is calculated. Moreover, the magnitude of separation of two bands found in complexes of proton donors bonded with pyridine through hydrogen bond is discussed in relation of their donating powers.

1. Introduction

It is well known that absorption band of OH group markedly increases in intensity and half-band width as a result of hydrogen bond formation. Though for the explanation of the origin, from which the anomalous features of the associated band result, various models[1] have been proposed by many workers, any of them has little direct experimental evidence to justify it.

Since spectral line shape depends naturally on the mechanism (in condensed systems, involving intermolecular force) by which light is emitted or absorbed, by examining the shape of the associated band some informations are to be expected to be obtained about the cause of the anomalous band features due to hydrogen bonding.

In the previous papers[2)-4)], it was shown that the first overtone band of associated O–H stretching vibration is separable into two components, both of

1) S. Bratoz and D. Hadzi: J. Chem. Phys. **27** (1955) 991.
2) Y. Sato and S. Nagakura: Science of Light **4** (1955) 120.
3) Y. Sato: Science of Light **6** (1957) 108.
4) Y. Sato: Science of Light **6** (1957) 69.

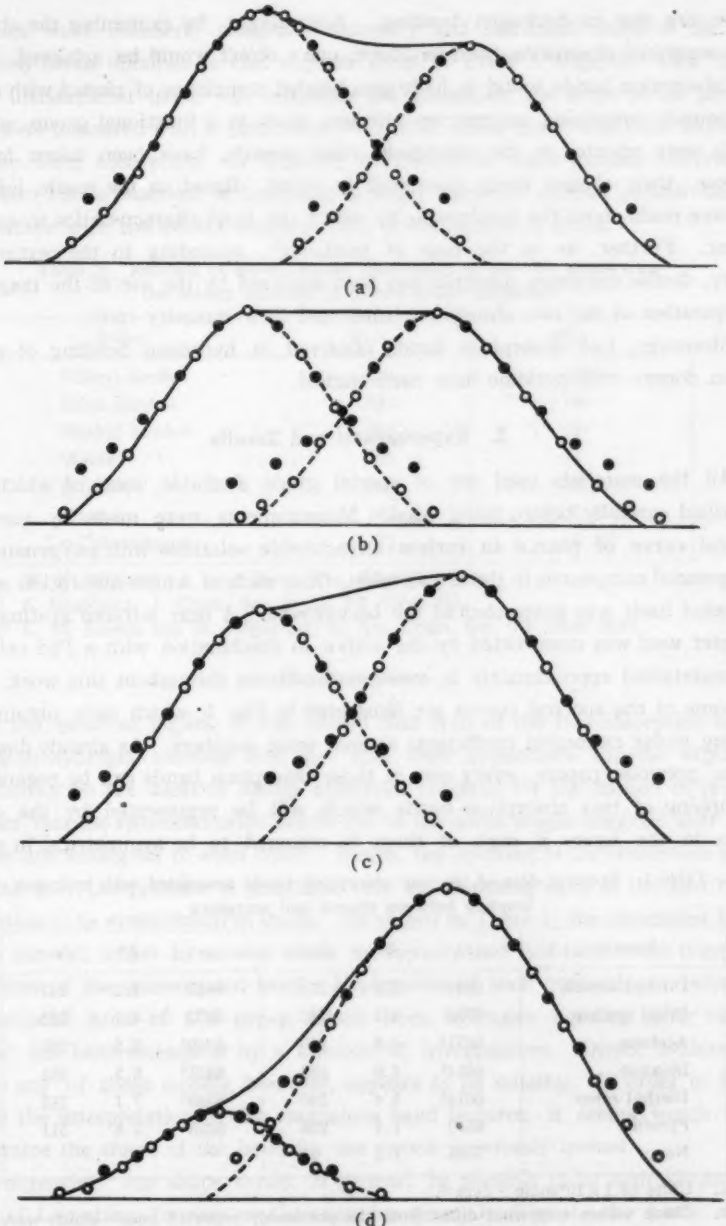

Fig. 1. Infrared spectra of complexes of phenol bonded with:
(a) diethyl ketone; (b) ethyl acetate; (c) acetone; (d) pyridine.

which are due to hydrogen bonding. Accordingly, by examining the shape of such separated absorption band as above, one's object would be achieved. Then two absorption bands found in hydrogen bonded complexes of phenol with several compounds containing oxygen or nitrogen atom as a functional group, some of which were reported in the previously cited paper[2], have been taken for this purpose, their shapes being examined in detail. Based on the result, inference has been made about the mechanism by which the band characteristics in question appear. Further, as in the case of methanol[4], according to the perturbation theory, double minimum potential has been analyzed by the use of the magnitude of separation of the two absorption bands and their intensity ratio.

Moreover, two absorption bands observed in hydrogen bonding of various proton donors with pyridine have been studied.

2. Experimental and Results

All the materials used are of special grade available, some of which were redistilled carefully before being used. Measurements were made by recording spectral curve of phenol in carbon tetrachloride solutions with oxygenated and nitrogenated compounds in the 1.5 μ region, from each of which absorption spectra of phenol itself was subtracted as the background. A near infrared grating spectrometer used was constructed by the author in combination with a PbS cell, and was maintained approximately in constant conditions throughout this work.

Some of the spectral curves are illustrated in Fig. 1, which were obtained by plotting molar extinction coefficients against wave numbers. As already discussed in the previous papers, every one of these absorption bands can be regarded as overlapping of two absorption bands which will be represented by the dotted curves in the figure if each of them is assumed to be symmetrical in shape.

Table 1. Spectral data of the two absorption bands associated with hydrogen bonding between phenol and acceptors

Acceptor	ν_1	A[a]	$\Delta\nu_{1/2}$	ν_2	A[a]	$\Delta\nu_{1/2}$
Diethyl ketone	6684	5.3	291	6423	4.2	247
Ethyl acetate	6734	4.1	283	6473	4.1	283
Acetone	6631[b]	4.5	270	6369[b]	5.5	260
Dioxane	6614[b]	4.9	239	6431[b]	5.5	261
Diethyl ether	6612[b]	3.4	240	6349[b]	7.1	312
Pyridine	6510	1.4	208	6223	7.6	311
None	7045	1.5	43			

a: Units of 1×10^3 mole^{-1} l cm^{-2}.

b: These values somewhat differ from the previously reported ones[1] which were obtained without subtracting the absorption band of phenol.

Maximum wave numbers, integrated intensity and half-band width of the two absorption bands obtained in this way are listed in Table 1 together with those of the unassociated band. In obtaining the intensities, the areas of the plotted curves were measured with a planimeter. In most cases, there was little difficulty with the wing absorption. In Table 2, a relation of wave number differences of the two bands observed in hydrogen bonding between various proton donors and pyridine with the acidity constant pK_a of the donors is given.

Table 2. Relation of wave number differences of the two bands with the acidity constant of proton donor molecules

Donor	$\Delta\nu_{12}$	pK_a
t-Butyl alcohol	264	19[a]
Ethyl alcohol	323	18[a]
Methyl alcohol	404	16[a]
Water	395	14
p-Cresol	285	10.2[b]
Phenol	287	9.95[c]
o-Chlorophenol	272	8.42[b]

a: W. K. McEwen: J. Am. Chem. Soc. **58** (1936) 1124.
b: S. Nagakura: J. Chem. Soc. Japan **75** (1954) 891.
c: C. M. Judson and M. Kilpatrick: J. Am. Chem. Soc. **71** (1949) 3110.

3. Discussions

In the previous papers, it was shown that both of the two absorption bands are due to hydrogen bonding and also that their appearance can be explained satisfactorily on the basis of double minimum potential for the motion of proton. The fact that the two absorption bands are of the same origin suggests that their features are analogous to each other. Hence, the splitting of the absorption bands into the two components is justifiable only by supposing each of the two bands in question to be symmetrical in shape. As shown in Table 1, the associated bands are, in general, larger by several times in intensity and half-band width compared with those of the unassociated band. Explanation of such predominant behaviors of associated band of OH group arisen from hydrogen bonding using various models[1] has been attempted by a number of investigators. Direct evidence to justify any of these models, however, appears to be missing. In order to find a clue to the interpretation of the anomalous band features, it seems worth while to examine the shape of the band for the reason previously quoted.

Symmetrical line shape would, in general, be possible to be approximated by either of Lorentzian formula or Gaussian function. In Fig. 1, the black circles indicate the values calculated by Lorentzian formula, i.e., $\log I_0/I \propto a/(\nu-\nu_{max})^2+b^2$,

and the white circles by Gaussian function, i.e., $\log I_0/I \propto \exp(-\alpha(\nu-\nu_{max})^2)$. As clearly seen in the figure, both of the shapes of the two bands are characterized in fair approximation by Gaussian model with a value of α listed in Table 3, wherease in Lorentzian model the calculated values are off the bands, especially in the wings.

Table 3. Comparison of calculated and experimental vulues

Acceptor	α	$\alpha'\beta^2$
Diethyl ketone	3.8×10^{-5}	2.2×10^{-5}
Ethyl acetate	4.2 〃	2.3 〃
Acetone	4.0 〃	1.8 〃
Dioxane	5.3 〃	2.3 〃
Diethyl ether	5.0 〃	2.1 〃
Pyridine	4.6×10^{-4}	7.5×10^{-4}

Neutron diffraction studies[5),6)] on hydrogen bond suggest that O..O vibrations in O–H..O hydrogen bonded systems are of considerable large amplitudes. Since the anomalous band features under consideration may be then considered to result from distribution of the O..O distance[7)], let us calculate the factor which is regarded to determine the band shape of such a model. Justification of the above hypothesis will be assured by the following descriptions.

The O..O vibrational frequency has been observed as 210 cm^{-1}.[8)] for ice on Raman spectrum. Now the hydrogen bond energies for the phenoldioxane and -ethyl acetate complexes formed through hydrogen bond are 4.8 kcal/mole and 4.7 kcal/mole respectively[9)], these values being very close to the energy for ice of 4.8 kcal/mole. In addition, the O..O equlibrium distance in the complexes is considered to be nearly equal to that in ice from plot of X–H frequency versus X–H...Y distance, which was given by Nakamoto et al.[10)] in their studies on strong hydrogen bonds in crystals. Accordingly, the feature of the potential energy curves for the O..O motion of the hydrogen bonds in the complexes is to be similar to that for ice, which requires that their O..O vibrational frequencies are considerably close to the frequency in ice described above. By comparing such O..O frequency with the O–H stretching frequency of 3600 cm^{-1}, it is seen

5) G. E. Bacon and N. A. Curry: Acta Cryst. **9** (1956) 82.
6) G. E. Bacon and N. A. Curry: Proc. Roy. Soc. **A235** (1956) 552.
7) Lippincott and Schroeder briefly mentioned about the question in their paper: J. Chem. Phys. **23** (1955) 1099.
8) P. C. Cross, J. Burnham and P. A. Leighton: J. Am. Chem. Soc. **77** (1937) 1134.
9) S. Nagakura: J. Chem. Soc. Japan **74** (1953) 153.
10) K. Nakamoto, M. Margashes and R. E. Rundle: J. Am. Chem. Soc. **77** (1955) 6480.

that an adiabatic approximation could be accepted. Under such circumstances, the intensity of the associated band is to be obtained by integrating the product of probability distribution of finding the oscillator in a O..O distance and transition probability, the latter of which is determined from double minimum potential corresponding to the O..O distance. Provided that the transition probability remains approximately unchanged in variation of the O..O distance, the intensity distribution under consideration is to be determined only by the probability distribution of the O..O distance. If anharmonicity is neglected, the probability distribution is given by the square of absolute value of eigenfunction which belongs to the vibrationless state corresponding to the potential curve for the oscillator, i.e., by $|\Psi_0|^2 \propto \exp(-\alpha'(r-r_e)^2)$ where r_e is the O..O equlibrium distance and $\alpha' = 4\pi^2\mu\nu_{0\ldots0}/h$, in which μ is the reduced mass of the pair of molecules forming hydrogen bond, $\nu_{0\ldots0}$ the O..O vibrational frequency. In straightforward calculation, distribution in excited states has to be taken into consideration together with the anharmonicity. In this case, the probability distribution is represented by $\Sigma_v|\Psi_v|^2 \exp(-E_v/kT)/\Sigma_v \exp(-E_v/kT)$. Suppose $(r-r_e)=\beta(\nu-\nu_{max})$, in which the proportionality constant β is taken from the curve given by Nakamoto et al.[10] as follows. Since the O..O and O...N distances for the hydrogen bonds under consideration appear to be intermediate between 2.7 A and 2.8 A, β would be possible to be taken as the average value of gradients between the two corresponding points on the curve. Making use of the above relation between r and ν, we have $\exp(-\alpha(r-r_e)^2) \doteqdot \exp(-\alpha'\beta^2(\nu-\nu_{max})^2)$, in which the constant $\alpha'\beta^2$ can be obtained by calculation. Values of the $\alpha'\beta^2$ obtained in this way are also shown in Table 3. It is surprising that the agreement between $\alpha'\beta^2$ and α is considerably good in spite of various assumptions involved in the process of this calculation. From such a fact it would probably be reasonable to interpret that the anomalous behaviors of the associated band result mainly from the distribution of the O..O distance*.

Next, plotting the magnitude of the separation and the ratio of maximum extinction coefficients of the two bands against the basicity constant, which is logarithm of the ratio of dissociation constant in aqueous solution and dissociation constant of water itself. These values, except for dioxane and pyridine[11], were calculated from the experimental formula given by Gordy and Stanford[12] in their paper. According to their results, the basicity constant of dioxane should agree

11) D. H. McDaniel and H. C. Brown: J. Am. Chem. Soc. **77** (1956) 3756.

12) W. Gordy and S. C. Stanford: J. Chem. Phys. **9** (1941) 204.

* For the intensity anomaly, the increment of the effective charge suggested by Tsubomura, J. Chem. Phys., **24** (1956) 927 is further to be taken into account.

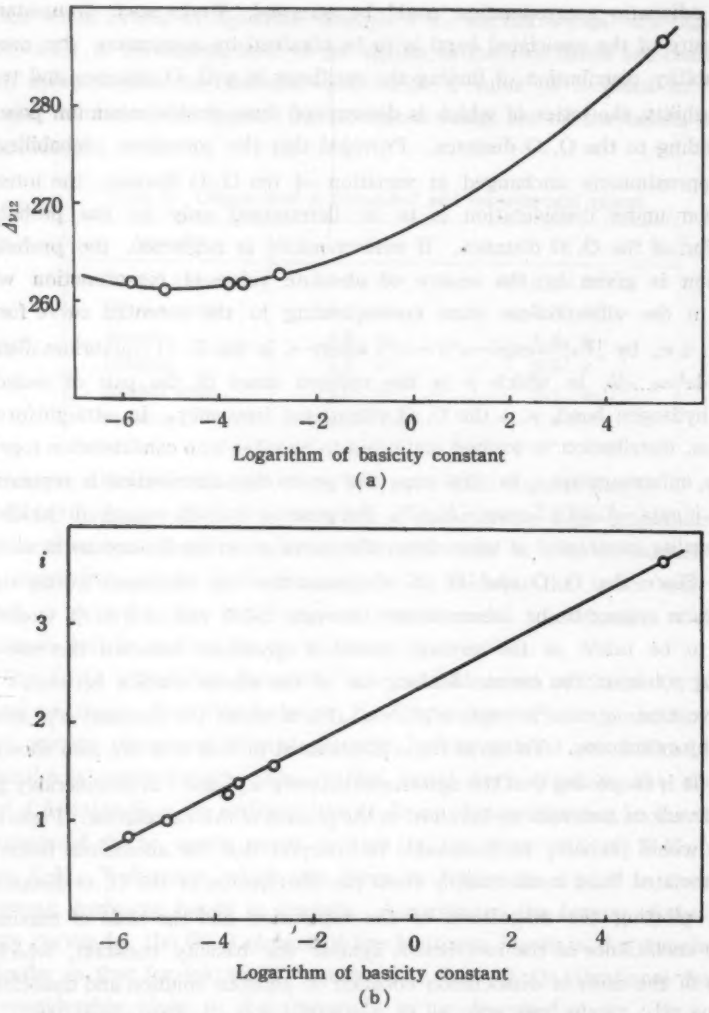

Fig. 2. Relations of the basicity constant of proton acceptor molecules with: (a) the magnitude of separation and (b) intensity ratio of the two bands.

with that of acetone, whereas the former estimated from Fig. 2 is slightly larger than the latter, which may be expected from comparison of their ionization potentials. As already pointed out in the case of methanol, both of these two quantities vary charateristically with the changing of the basicity constant of the acceptor molecule. Namely, as the basicity increases, the intensity of the

shorter wavelength band decreases and that of the longer wavelength band increases, the two being almost equal in the case of ethyl acetate. On the other hand, the magnitude of the separation of the two bands gradually increases for both of the stronger and weaker bases than ethyl acetate for which it is the smallest. These characteristic behaviors can clearly be explained on the basis of the double minimum potential as reasoned below.

Two vibrational levels, related to the infrared absorption under consideration corresponding to the minima, can perturb each other by tunneling through potential barrier, which results in producing perturbed levels

$$E_{1,2}=\frac{1}{2}(E_1^0+E_2^0)\pm\frac{1}{2}\sqrt{4|W_{12}|^2+\Delta^2}, \tag{1}$$

where E_1^0 and E_2^0 are the unperturbed energies. The eigenfunctions of the resulting two states can be shown to be the following mixtures of the zero approximation eigenfunctions φ_1^0 and φ_2^0:

$$\begin{aligned}\Psi_1&=a\varphi_1^0+b\varphi_2^0\\ \Psi_2&=a\varphi_1^0-b\varphi_2^0.\end{aligned} \tag{2}$$

The coefficients a and b in the above equations are respectively given by

$$\begin{aligned}a&=\sqrt{4|W_{12}|^2+\Delta^2}+\Delta/\sqrt{4|W_{12}|^2+\Delta^2}\\ b&=\sqrt{4|W_{12}|^2+\Delta^2}-\Delta/\sqrt{4|W_{12}|^2+\Delta^2},\end{aligned} \tag{3}$$

where W_{12} represents the matrix element of the perturbation function, Δ the magnitude of the separation of the unperturbed energies. In consequence of applying a similar method as in the case of methanol, the intensity ratio is given as

$$i\simeq b^2/a^2=\Delta E-\Delta/\Delta E+\Delta, \tag{4}$$

in which ΔE is the magnitude of the separation of the perturbed levels and is expressed by

$$\Delta E=\sqrt{4|W_{12}|^2+\Delta^2}. \tag{5}$$

When Δ is calculated from Eq. (4) using the experimentally obtained i and ΔE, it would be more rational to examine i by taking the intensity ratio of the two bands corresponding to the O...O equlibrium distance rather than that of the two bands shown in Fig. 1. The former can be approximately given by a ratio of products of respective maximum extinction coefficients and half-band widths, of which the half-band width ratio is assumed to be nearly equal to that listed in Table 1. By such means, Δ and further the unperturbed energies are obtained. The coefficients a and b are also evaluated from Eqs. (5) and (3). All these values are summarized in Table 4. In Fig. 3, plots of the coefficients a's in the mixture of the zero approximation eigenfunctions and of the unperturbed energies E_1^0's corresponding to the potential curve of OH group against the

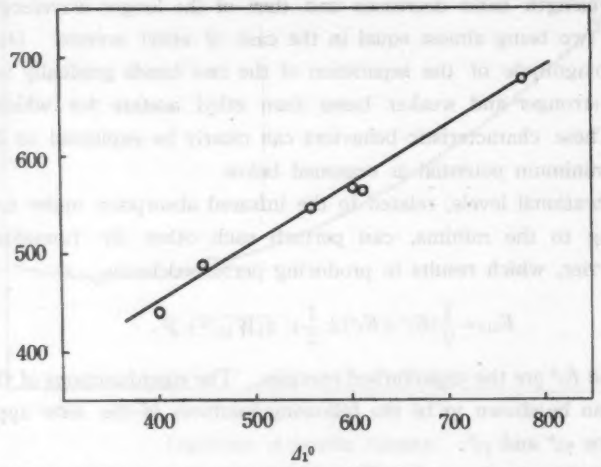

Fig. 3. Relation of the average value of the shifts of the two bands with the shift of the first unperturbed level.

Table 4. Relations of the proton acceptors to separations of the two bands and of the unperturbed levels, the first unperturbed level, and coefficient in mixtures of zero approximation sigenfunctions.

Acceptor	$\Delta\nu_{12}$	Δ	$\lvert W_{12}\rvert$	E^0_1	a
Diethyl ketone	262	41	129	6679	0.65
Ethyl acetate	261	0	130	6604	0.70
Acetone	262	22	130	6489	0.74
Dioxane	262	58	128	6443	0.76
Diethyl ether	263	94	123	6434	0.82
Pyridine	287	198	108	6268	0.92

basicity constants are given. From the curve of E_1^0, the trend can be seen of the potential curve being modified by the hydrogen bond formation, i.e., becoming shallow by the elongation of the OH bond length. Rate of this modification is comparatively large for weak base and considerably small for strong base, which reflects the possibility of the appearance of shorter wavelength band with strong base such as amines. In Fig. 4, plots are given of the average value of the shifts of the two bands from the free OH band against the shift of the first unperturbed level. A linear relationship are seen between them, as poined out in the case of methanol.

By making use of the results given in Table 4, let us calculate the time required for a proton to transfer from one minimum potential to the other. As a

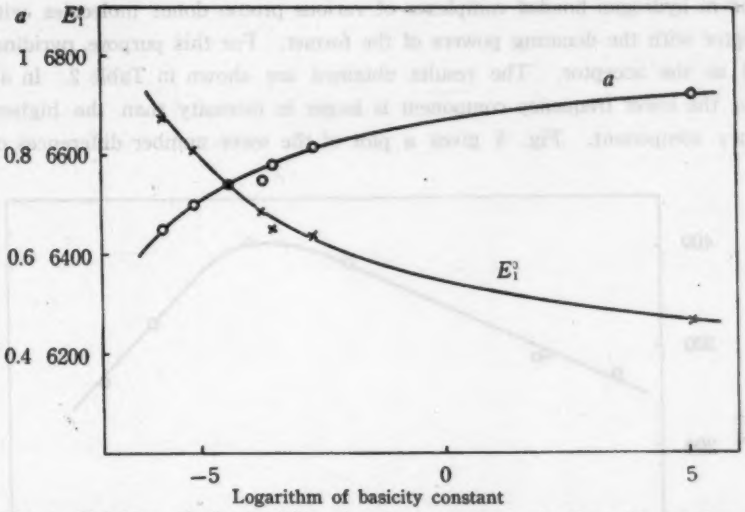

Fig. 4. Relations of the basicity of proton acceptor molecules with the first unperturbed energy E_1^0 and coefficient a in mixing of zero approximation eigenfunctions.

solution of the Schrödinger wave equation involving time $i\hbar\partial\Psi/\partial t=H\Psi$, where H is Hamiltonian for the proton,

$$\Psi=c_1\cdot\exp(-iE_1t/h)\Psi_1+c_2\exp(-iE_2t/h)\Psi_2 \qquad (6)$$

will be taken. By substituting Eq. (1) into the above equation, and considering the initial condition $\Psi=\varphi_1^0$ at $t=0$, the coefficients c_1 and c_2 can be determined. If φ_1^0 and φ_2^0 are orthogonal to each other, probabilities of the proton occupying φ_1^0 and φ_2^0 at a time t are expressed by the squares of absolute values of the respective coefficients of φ_1^0 and φ_2^0 in Eq. (6). Here the life-time of the proton transfer can be estimated from the following formula

$$P_2(t)/P_1(t)=1/2, \qquad (7)$$

where $P_1(t)$ and $P_2(t)$ are the probabilities just described above. For example, with ethyl acetate, the period is of the order of 10^{-14} sec. The life-time of the excited vibrational state with respect to radiation appears to be of the order of 10^{-8} sec., which means numerous proton transfers. The line broadening due to tunnel effect would therefore be neglected. Moreover, the period is less than the time required for readjustment of solvent orientation which is of the order of of 10^{-11} sec.[13]; the proton transfer can not be followed by the solvent reorientation.

Finally, it is of interest to study the relationship of the two absorption bands

13) D. H. Whiffen: Quart. Revs. **4** (1950) 131.

found in hydrogen bonded complexes of various proton donor molecules with an acceptor with the donating powers of the former. For this purpose, pyridine was used as the acceptor. The results obtained are shown in Table 2. In all the cases, the lower frequency component is larger in intensity than the higher frequency component. Fig. 5 gives a plot of the wave number differences of the

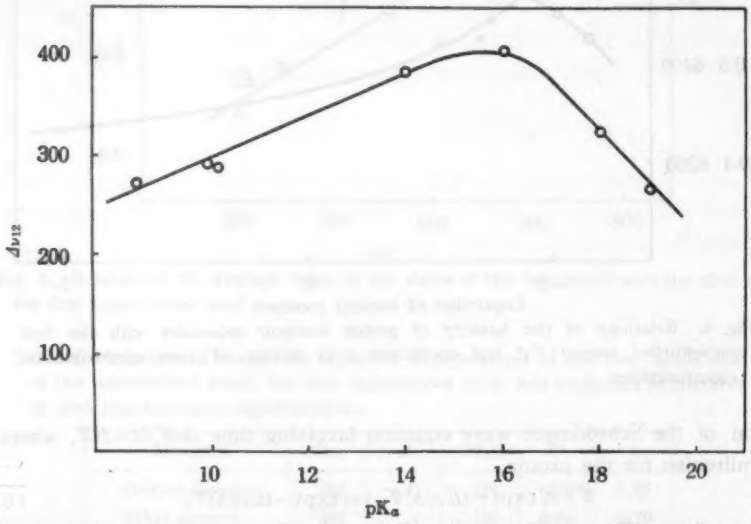

Fig. 5. Plot of the wave number difference of the two bands vs. the acidity constant of the donors.

two bands against the acidity constants of the donor molecules. The acidity constant is regarded as a measure of the proton donating power (Bronsted acid). As clearly seen from the results, the magnitude of the separation of the two bands is the largest for methanol, decreasing for acids weaker and stronger than methanol. Such a behavior would also be understood on the basis of the modification of double minimum potential by the hydrogen bond formation.

Acknowledgement

The author wishes to express his sincere thanks to Professor Y. Fujioka for his guidance and continued encouragement, to Professor H. Ootsuka for his deep interest, to Professors M. Toda of Department of Physics, M. Seya and S. Nagakura of University of Tokyo for their valuable advice, and to Assi. Prof. S. Hachisu for his very valuable help offered throughout this work.

CONTENTS

Grating Mounting for Vacuum Ultraviolet Monochromator.....R. ONAKA 23

Brightness Standard for Night Airglow Photometers of OI λ5577 .....
..... R. ONAKA and M. NAKAMURA 28

Reflectivity Curves by Multiple Layers of Alternating Refractive Indices on Image Basis and Lippmann Photography 33
.....M. IWATA, S. KATSUBE and T. FUKUDA

Current Dependence of Decay of Metastable Mercury Atoms in Argon-Mercury Discharge Afterglows .....M. YOKOYAMA 42

Anomalous Band Features of OH Groups due to Hydrogen Bonding..Y. SATO 56